Research article

JGS
Journal of the Geological Society

Published online October 23, 2019 https://doi.org/10.1144/jgs2018-167 | Vol. 177 | 2020 | pp. 395–411

Cenozoic tectonic evolution of southeastern Thailand derived from low-temperature thermochronology

Simon Nachtergaele[1]*, Stijn Glorie[2], Christopher Morley[3], Punya Charusiri[4], Pitsanupong Kanjanapayont[4], Pieter Vermeesch[5], Andrew Carter[5], Gerben Van Ranst[1] & Johan De Grave[1]

[1] Laboratory for Mineralogy and Petrology, Department of Geology, Ghent University, 9000, Ghent, Belgium
[2] Centre for Tectonics, Resources and Exploration (TRaX), Department of Earth Sciences, School of Physical Sciences, University of Adelaide, 5005 Adelaide, SA, Australia
[3] Petroleum Geophysics Program, Department of Geological Sciences, Chiang Mai University, Chiang Mai, Thailand
[4] Basin Analysis and Structural Evolution Special Task force for Activating Research (BASE STAR), Department of Geology, Chulalongkorn University, Bangkok, Thailand
[5] Department of Earth & Planetary Sciences, University College London, WC1E 6BS London, UK

SN, 0000-0002-5451-4627; CM, 0000-0002-6075-9022; PC, 0000-0002-1767-3936; PV, 0000-0003-3404-1209; AC, 0000-0002-0090-5868; GV, 0000-0002-0664-4777

* Correspondence: simon.nachtergaele@ugent.be

Abstract: Low-temperature thermochronological techniques, specifically apatite (U–Th)/He and apatite fission-track dating, were used to reconstruct the thermal history of southeastern Thailand. This area is intersected by vast and complex fault networks related to the Cenozoic Mae Ping and Three Pagodas Faults. These were identified from satellite imagery and confirmed by field observations. New apatite fission-track and apatite (U–Th)/He data were collected from crystalline basement blocks within these fault networks. Ages obtained range from 48 to 24 Ma, with most of the samples clustering between 36 and 24 Ma. Thermal history modelling indicates late Eocene–Oligocene exhumation of the exposed granitic and metamorphic basement rocks in southeastern Thailand. Exhumation was regional and was contemporaneous with sinistral fault activity during the late Eocene–early Oligocene along the Mae Ping Fault and Three Pagodas Fault. Moreover, this exhumation occurred coevally with a synrift phase of intracontinental offshore rift basin and half-graben basin development in the eastern Gulf of Thailand. The phase of exhumation ended in the early Miocene, as a result of the changing plate-tectonic forces along the complex plate boundaries of Sundaland.

Supplementary material: AFT data, radial plots and the detailed procedure of thermal history modelling are available at https://doi.org/10.6084/m9.figshare.c.4633064

Received 5 September 2018; **revised** 15 July 2019; **accepted** 8 August 2019

Southeastern Thailand is one of the critical areas for understanding the Indosinian Orogeny because it contains good exposures of all three major tectonic terranes (Sibumasu, Sukhothai–Chantaburi, Indochina) and their intervening suture zones (Inthanon Zone, Nan-Sa Kaew suture) (Figs 1 and 2). Post-collision extension of uncertain age has also affected the area. Late Cretaceous–Cenozoic tectonics is particularly well expressed in this area along an extensive network of strike-slip faults. In western Thailand the Mae Ping and Three Pagodas Fault zones (Figs 2 and 3) are two major NW–SE-trending, poorly dated strike-slip fault zones that have undergone sinistral motion at least during the late Eocene, with motion ending in the early Oligocene (Lacassin *et al*. 1997). These fault zones have possibly been affected by Late Cretaceous–Paleogene transpressional deformation, and later movements related to escape tectonics, which include early sinistral motion and later dextral motion (Morley *et al*. 2011; Morley 2012). Encountering southeastern Thailand these strike-slip fault zones become broader, and exhibit a variety of geometries, including splays, horsetails and duplexes (e.g. Morley 2002; Morley *et al*. 2011, 2007, 2004). The region also borders the Gulf of Thailand, which has undergone a diachronous phase of rifting (Eocene–Miocene), followed by diachronous Miocene–Recent post-rift subsidence. Upton (1999) identified regional uplift-induced denudation or basement exhumation trends regionally across Thailand using apatite fission-track (AFT) data (supplementary material, Appendix 1). Upton (1999) showed that most exhumation was of Cenozoic age, being generally older in the east (Paleogene) and younger in the west (Neogene) (supplementary material, Appendix 1). However, southeastern Thailand was very undersampled in his study (Fig. 3), hence the exhumation history of this region is poorly constrained. The issues concerning southeastern Thailand that require an understanding of the exhumation history include the following. (1) What is the timing of the strike-slip faults and how does it compare with activity further west and east? (2) What effect did Cenozoic rifting and post-rift subsidence in the Gulf of Thailand have on exhumation of the adjacent onshore areas? (3) What are the processes that contributed to exhumation of the Indosinian suture zones to the surface? (4) What is the influence of the Indosinian Orogeny inherited structures on the basin formation history, both on- and offshore, and how are they related? Understanding the exhumation history contributes a piece of information to the regional structural geological picture, which is necessary to gain deeper insights into the complex evolution of driving forces and their tectonic intraplate consequences and deformation history in the Sunda plate (Sundaland) during the Cenozoic (Fig. 1). Furthermore, the Sunda plate is a prime example of how rift basins and spreading centres develop diachronously and suddenly stop owing to a changing intraplate stress field.

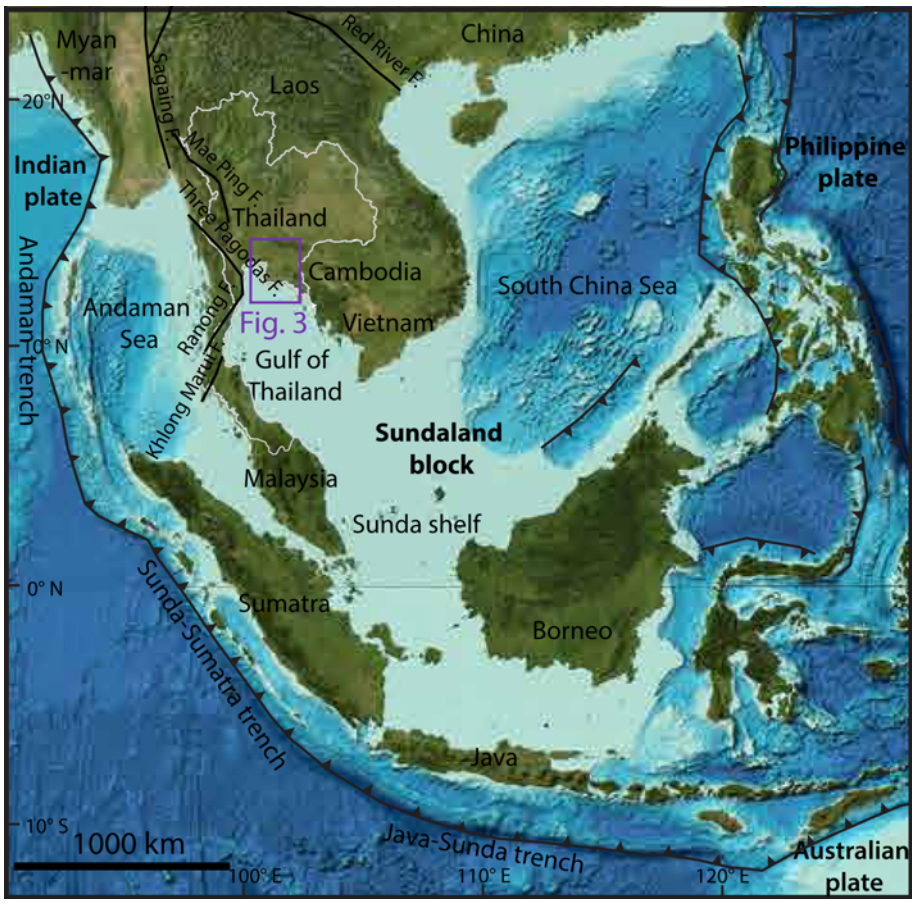

Fig. 1. Overview of SE Asia in its plate-tectonic context. The major strike-slip faults, trenches and tectonic plates are indicated in black. The national borders of Thailand are indicated in white. The purple rectangle indicates the location of Fig. 3. Adapted from Simons *et al.* (2007) and Metcalfe (2013).

This study combines observations from fieldwork with low-temperature thermochronology to reconstruct the thermal history of southeastern Thailand with emphasis on documenting the cooling of the basement rocks adjacent to the aforementioned faults in an absolute time frame. Here, we date the cooling of mainly granitoid basement through the upper crustal isotherms as a result of denudation of the overlying rock column; this denudation was caused by erosion or tectonic exhumation. The cooling history of the basement, and in particular the targeted deformed granitoids and metamorphosed rocks, places new constraints on the activity of the Mae Ping and Three Pagodas Faults as a response to regional or local plate-tectonic forces. These long-lived strike-slip faults functioned as the principal crustal strain accommodators during phases of compressional and extensional stresses in northwestern Sundaland.

Geological setting

Southeastern Thailand comprises many low-relief areas (100 m elevation or less) punctuated by NW–SE- to NNW–SSE-trending linear hills and ridges, where Cenozoic strike-slip faults have influenced the trends, and more oval, high-relief areas that are related to more erosion-resistant granitic plutons (Fig. 3). The highest relief is associated with the Khao Soi Dao Triassic pluton north of Chantaburi, where the highest peak exceeds 1600 m, but in general relief is less than 1000 m, and ridges in Paleozoic and Mesozoic sedimentary, low-grade metamorphic and volcanic units are commonly 300–500 m high. The study area is on the margin of the Gulf of Thailand, which is currently undergoing post-rift subsidence. The overall topographic expression suggests a region of previous uplift, with strong strike-slip control, that has been considerably eroded. Slow, continuing subsidence has resulted in gradual infilling and onlap of the topography by recently deposited sediments.

Assembly of the basement units of Thailand

Our study area (Fig. 3) comprises three north–south-oriented tectonic domains, which now form the basement of Thailand: Indochina in the east, Sibumasu (including the Inthanon Zone) to the west and the Sukhothai Arc in the centre (e.g. Metcalfe 2011) (Fig. 2a). These terranes underwent several phases of granite intrusion, as a result of their accretionary history into the Sundaland collage; for example, during the Triassic–Early Jurassic Indosinian Orogeny (Metcalfe 1996). These granite belts are traditionally subdivided in north–south-oriented Eastern, Central and Western Granite Provinces and separated by suture zones (Hutchison 1975, 1977, 2007; Mitchell 1977) (Fig. 2a). The Indochina terrane rifted away from Gondwana during the Devonian and collided on its current northeastern side with South China in the Early Triassic (Lepvrier *et al.* 2004). Since the late Carboniferous–early Permian, the Nan-Sa Kaeo back-arc basin lay on the western side of the Indochina terrane, separating the Cathaysian Sukhothai arc from Indochina (Metcalfe 2013). The Nan-Sa Kaeo back-arc basin closed in the Early–Middle Triassic during the collision of the Sukhothai Arc with Indochina (Sone & Metcalfe 2008; Metcalfe 2013) as the Paleo-Tethys Ocean continued to close. The back-arc basin preserved early Permian to early–middle Triassic pelagic chert deposits, representative of deep-water environment (Sone *et al.* 2012). In our study area, remnants of these sequences with ophiolitic mélange such as bedded cherts, limestones, serpentinites, gabbros and pillow lavas are preserved in the (Nan-)Sa Kaeo (or Sra Kaew) suture zone (Hutchison 1975; Metcalfe 2000; Sone & Metcalfe 2008) (Figs 2b and 5). West of the Nan-Sa Kaeo suture zone lies the Sukhothai volcanic arc, which is in turn separated from the adjoining tectonic unit (i.e. the Sibumasu block) by the so-called Klaeng tectonic line (Sone *et al.* 2012) (Figs 2a, b and 5). Sibumasu was separated from Gondwana in the late Early Permian and collided with the Sukhothai arc in the late Triassic–early Jurassic

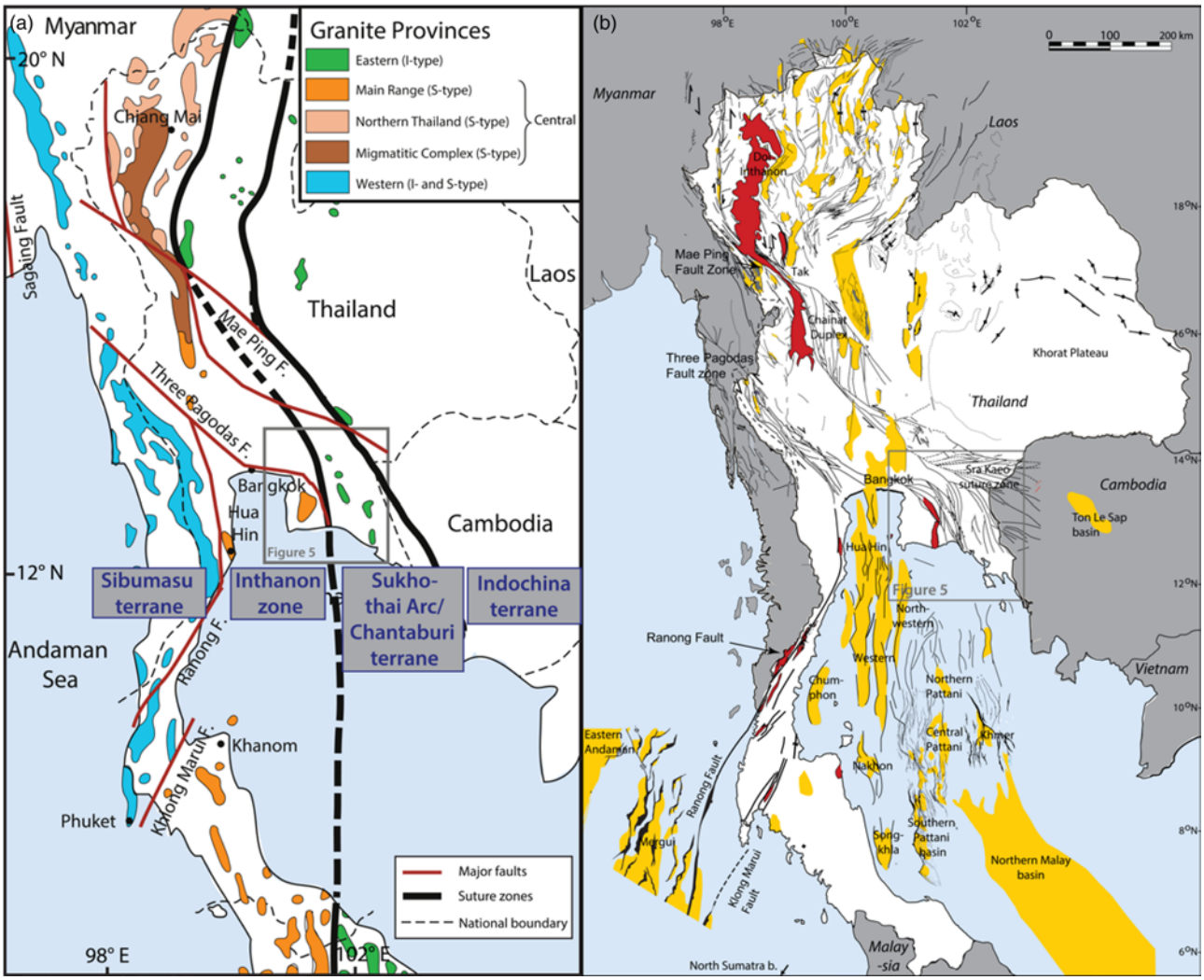

Fig. 2. (**a**) Tectonic subdivision and the distinct granite provinces in Thailand and surrounding countries. Major faults discussed in the text are indicated in red. The suture zones between terranes are also shown. Adapted from Gardiner *et al*. (2016). (**b**) Structural map of Thailand with the indication of the complex fault network (black lines), basins (yellow), metamorphic core complexes (red) and Cenozoic folds in the Khorat Group. The study area, illustrated in Fig. 5, is indicated by a grey rectangle. Adapted from Morley *et al*. (2011) and Morley (2015).

(e.g. Metcalfe 2013; Morley 2018) during the main phase of the Indosinian Orogeny and final Paleo-Tethys Ocean closure. The Inthanon Zone is thrust over the eastern part of the Sibumasu and represents the accretionary complex of the Indosinian Orogeny (Barber *et al*. 2011; Ridd 2015). This accretionary complex underwent east–west compression and westward thrusting as nappes during Indosinian accretion of Sibumasu (Ridd 2015). In eastern Thailand the Sibumasu block is located to the west of the Three Pagodas Fault and Khlong Marui Fault zone (Fig. 2a).

Long-lasting subduction of Paleo-Tethyan oceanic lithosphere from the Middle Devonian until the early Late Triassic (Sone & Metcalfe 2008) beneath Indochina is characterized by island arc and back-arc basin and magmatic arc development, which resulted in a belt of north–south-aligned I-type (mantle-derived) granites (Eastern Granite Province) exposed across the Sukhothai arc and Indochina alike (Cobbing 2011; Searle *et al*. 2012; Metcalfe 2013). These I-type granites of the Eastern Granite Province are exposed in our study area (Figs 2 and 5) and typically yield late Triassic zircon U–Pb ages (Qian *et al*. 2017, and references therein). The Klaeng Fault 'cryptic suture zone' contains mylonitic gneisses and migmatites (Sone *et al*. 2012), which seem to show peak metamorphism ages of 234 ± 3 and 232 ± 2 Ma (Geard 2008) and constrain the collision and final closure of the Paleo-Tethyan Ocean (Gardiner *et al*. 2016; Qian *et al*. 2017).

A large volume of S-type granites (Central Granite Province) intruded the Inthanon Zone when Sibumasu collided with the Sukhothai arc in the middle–early Late Triassic (Metcalfe 2013). The Central Granite Province covers the largest part of present-day Thailand and is exposed from the northern border of Thailand with Myanmar to the southern part of Thailand at its border with Malaysia (Cobbing 2011) (Figs 1 and 2). The part of the Central Granite Province located in our study area in southeastern Thailand is called the Main Range Granite Province, where it comprises the plutons of Rayong, Chonburi and Ban Na Cham (Cobbing 2011). These granitoids are one of the main lithologies targeted for sampling in this study.

The Cretaceous S- and I-type granites of the Western Granite Province are located in the Sibumasu block (or Mogok–Mandalay–Mergui belt; Gardiner *et al*. 2015) to the west of our study area in Peninsular Thailand and Myanmar (Cobbing 1992; Gardiner *et al*. 2015).

In general, the granites that intruded into the Indochina terrane have more juvenile geochemical and isotopic characteristics, as indicated by positive zircon εNd values, whereas the Sibumasu block and the Inthanon Zone provide negative zircon εNd values, implying that the source for the latter granitoids was more evolved, and possibly pertains to recycled crust (Qian *et al*. 2017; Dew *et al*. 2018*a*, *b*). The Sukhothai Arc has intermediate zircon εNd values, indicative of a more hybrid crustal source (Dew *et al*. 2018*a*).

Late Mesozoic–Cenozoic tectonic evolution

During the Late Cretaceous–Eocene, an Andean-type margin developed in western Sundaland. Related events include the formation of suprasubduction-zone oceanic crust around 95 ± 2 Ma in the vicinity of the Andaman Islands (Pedersen *et al*. 2010; Pal 2011). Emplacement of large-scale I-type granite intrusions of Late Cretaceous–Paleogene age in the Wuntho–Popa magmatic arc occurred, together with aforementioned S-type granites in the Mogok–Mandalay–Mergui belt (i.e. in Sibumasu basement) (Gardiner *et al*. 2015). Whereas high-grade metamorphic complexes have yielded latest Cretaceous ages in the Doi Inthanon and Doi Suthep region (67–83 Ma) and the Lansang gneiss (70 Ma; Gardiner *et al*. 2016) (Fig. 2), peak metamorphism alongside the Three Pagodas Fault is Paleogene in age and occurred around 57–51 Ma in the Thabsila metamorphic complex (Fig. 2b; Nantasin *et al*. 2012). This metamorphism was accompanied by widespread I- and S-type granite emplacement in the Western Granite Province from the Late Cretaceous until the Eocene (e.g. Charusiri *et al*. 1993; Cobbing 2011). This late metamorphism and even associated anatexis is clearly expressed in the Khao Chao region of our study area (Kawakami *et al*. 2014).

$^{40}Ar/^{39}Ar$ analyses constrained the termination of ductile sinistral deformation on the Three Pagodas Fault in the latest Eocene (36–33 Ma) and the termination of ductile sinistral deformation along the Mae Ping Fault zone in the earliest Oligocene (33–30 Ma) in western Thailand (Lacassin *et al*. 1997; Nantasin *et al*. 2012). This was followed by minor reactivation by dextral motion in the late Oligocene (Smith *et al*. 2007) or even an uplift-related event during the Oligocene–Miocene transition (*c.* 23 Ma) (Lacassin *et al*. 1997), resulting in the current geometry of the Chainat Duplex (Smith *et al*. 2007) (Figs 2b and 3). The southeastern continuation of these two NW–SE- to north–south-oriented faults coincides with our study area (Morley *et al*. 2011) (Figs 2b and 3). The Mae Ping Fault is thought to continue further eastwards and branches into numerous splays in Cambodia close to the Ton Le Sap basin (Ridd & Morley 2011; Morley 2012) and further to the SE into the Cuu Long basin, offshore Vietnam (Schmidt *et al*. 2019) (Fig. 2b). The Three Pagodas Fault zone south of Kanchanaburi splays into several trends including the north–south Ranong Fault and the more east–west trend that runs through Bangkok before curving to the NW–SE trend of the Klaeng Fault zone (Morley 2002; Ridd 2009) (Figs 2a, b and 3). The Ranong Fault shows episodic activity, with an early phase before the Late Cretaceous (*c.* 81 Ma), based on $^{40}Ar/^{39}Ar$ and zircon U–Pb dating (Watkinson *et al*. 2011; Kanjanapayont *et al*. 2012), and together with the Khlong Marui Fault underwent ductile dextral strike-slip shear from 47 to 43 Ma, followed by a phase of brittle sinistral reactivation from 37 to 30 Ma (Watkinson *et al*. 2011). Apatite fission-track data from Peninsular Thailand indicate final cooling through the isotherms at *c.* 23 Ma for the current basement blocks, with exposed granites and gneisses along the Ranong Fault zone (Upton 1999; Blomme 2013; Nachtergaele *et al*. 2017). Further south, in Malaysia, crustal thickening in the Paleogene was followed by rapid cooling in the Eocene–late Oligocene, based on apatite fission-track and apatite and zircon (U–Th)/He cooling ages (Krähenbuhl 1991; Cottam *et al*. 2013; Md Ali *et al*. 2016; François *et al*. 2017).

Geochronological information in southeastern Thailand is rather limited to the aforementioned high-grade metamorphic rocks in the Klaeng Fault zone (Geard 2008; Kanjanapayont *et al*. 2013; Kawakami *et al*. 2014). Structural geological data from our study area suggest Eocene sinistral ductile deformation in the high-grade metamorphic rocks in the Klaeng Fault zone area (Geard 2008; Kanjanapayont *et al*. 2013). The Klaeng Fault gneisses are crosscut by leucogranites, with a Late Cretaceous crystallization age (78.1 ± 0.7 Ma) (Cobbing 2011; Kanjanapayont *et al*. 2013). Sinistral ductile shearing post-dates leucogranites formed at 67 ± 1 and 72.1 ± 0.6 Ma (Kanjanapayont *et al*. 2013). The complex tectonic history of these mylonitic gneisses is further constrained by a U–Pb monazite age of 42.54 ± 0.88 Ma, and U–Pb titanite ages of 35.5 ± 3.1 and 37.8 ± 4.8 Ma (Geard 2008; Crow 2011). All geochronological and structural geological evidence suggests that the Klaeng tectonic line (bounding the Sibumasu block in the west and the Sukhothai Arc in the east) experienced a complex and protracted history of reactivation and metamorphism during the Late Cretaceous and Cenozoic (Ridd 2012; Sone *et al*. 2012).

Post-Indosinian structures of southeastern Thailand

Whereas evidence for strike-slip control is clear from satellite images and geological maps (e.g. Ridd & Morley 2011; Morley 2012; Fig. 3), there is little published documentation of the structures from outcrop (Morley 2012). However, one of the authors (C.M.) has found that strike-slip faults are commonly present in small, temporary exposures created while digging into hills for buildings or small aggregate quarries, all the way across the region from Chantaburi to north of Rayong (Fig. 4). Generally these are narrow, subvertical fault zones, marked by zones of cataclasis and gouge zones a few centimetres wide, and broader zones a few metres wide where bedding and/or foliations are subvertical and aligned parallel or subparallel to the fault zone (Fig. 4b). In Klaeng town a highly weathered NNW–SSE-trending sinistral strike-slip mylonite zone was (temporarily) exposed in a building site, supporting the existence of the Klaeng Fault, which is primarily a feature interpreted from remote sensing images. The best exposed, more permanent strike-slip fault-related exposures are along the coast, in the Cretaceous Khao Thalai red beds along the Khao Thalai Ridge (Thai Mai Fault) (Ridd & Morley 2011; Morley 2012). A quarry in the Khao Chao area shows a strand of the Klaeng Fault zone (Fig. 4c–f). This quarry exposes migmatites and leucogranites on the southern side of the fault, juxtaposed with amphibolites on the northern side (Fig. 4c and d). The fault zone is a narrow, brittle, transpressive zone, with chlorite extensively distributed within the fault zone. The biotite–garnet schists within the fault zone are strongly altered in part owing to surface weathering, and in part owing to fluid movement along the fault during deformation. In this case the brittle fault zone is later than the metamorphic fabric. The three terranes assembled during the Indosinian Orogeny are all present in southeastern Thailand, and are separated by two NNW–SSE-trending suture zones (Inthanon Zone and the Sa Kaeo suture; Sone *et al*. 2012). Therefore the study area for the low-temperature analyses in this work holds a key position with respect to the broader tectonic architecture. The contacts within the zones appear to be highly disrupted by the later strike-slip faults.

East of Rayong there is a north–south-trending, low-angle extensional mylonite zone several hundred metres thick, which has reworked the eastern margin of the large Triassic granite pluton complex that occupies much of the area between Rayong and Chonburi. In the hanging wall of the top-to-the-NE granite, mylonites are flanked by schists and Permo-Triassic sedimentary units. Unconformably overlying these units is a less-deformed red bed sequence, of equivalent age to the Khorat Group (Jurassic–Cretaceous; Geard 2008). The timing of extension is uncertain, and could range between the Latest Triassic and the Cenozoic. Major low-angle extensional events regionally are of Late Triassic age and younger (e.g. Late Triassic, basal Paleozoic, Inthanon area, northern Thailand; Late Cretaceous, Stong Metamorphic Complex, northern Malaysia; Eocene, Khanom area, southern Thailand, Morley *et al*. 2011; Late Oligocene–Early Miocene, for example, Doi Inthanon, northern Thailand; see review by Morley *et al*. 2011).

Cenozoic basin evolution in the Gulf of Thailand

During the development of the oblique Andean-type margin from the Late Cretaceous to the Eocene, the crust in the Gulf of Thailand and adjacent areas became overthickened and hot (Morley 2004, 2012; Palin *et al*. 2013; Gardiner *et al*. 2015). This overthickened crust in places experienced orogenic collapse in the late Eocene, leading to extension and basin development in the Gulf of Thailand. Conversely, onshore parts of Thailand still experienced transpressional deformation, related to major strike-slip fault activity in the late Eocene and Oligocene (Morley *et al*. 2011; Morley 2012; Pubellier & Morley 2014).

The offshore rift basins of the Gulf of Thailand are predominantly filled by continental deposits (Morley & Westaway 2006) attesting to the exhumation and erosion of adjoining continental basement blocks. Marine incursion periodically affected the Gulf of Thailand during the Miocene, and became more widespread and longer lived during the Pliocene–Recent (Morley & Westaway 2006). The basins of the Gulf of Thailand developed diachronously, whereby the basins located in the eastern Gulf of Thailand (i.e. northern Malay basin and Pattani basin; Fig. 2b) started to rift in the late Eocene and Oligocene and rifting ceased around the Oligocene–Miocene transition (*c.* 23 Ma), followed by the deposition of kilometres of post-rift sediments on top of this synrift section (Morley & Racey 2011). This resulted in a minimal thickness of 7 km for the Pattani and North Malay basin (Morley & Racey 2011). However, the main phase of basin development in the south of the Gulf of Thailand (i.e. Chumphon, Nakhon, Songkhla, Khmer, North Malay and Pattani; Fig. 2b) was in the Late Eocene, although in the deepest basins (i.e. North Malay and Pattani) it is problematic to observe the base of the sedimentary sections and biostratigraphic dating of the lowest stratigraphic levels lacks resolution (Heward *et al*. 2000; Morley & Racey 2011; Racey 2011; Morley 2015; Sautter *et al*. 2017).

In the western Gulf of Thailand, rifting initiated in the (late) Oligocene and continued in the early Miocene after rifting had already ceased in the eastern part of the gulf (Morley & Racey 2011). Besides the diachronous onset of rifting, these basins contain more 'anomalous' features, which were discussed by Morley (2015), such as (1) the occurrence of low-angle normal faults, (2) synrift episodes alternating with basin inversion, (3) rapid post-rift subsidence and (4) the occurrence of numerous, low-displacement post-rift faults. All of these anomalous features can be attributed to the characteristics of the underlying weak and hot crust in which they developed (Morley 2015). Lower crustal flow could explain the extreme thick post-rift sections in the Pattani and Malay basins in SE Asia, which accumulated up to 6 km and 12 km of syn- and post-rift sediments respectively (Morley & Westaway 2006).

Regional geological context of the Sunda plate

It has been suggested that a combination of stresses arising from collision zones (e.g. eastern Himalayas, Australia–Indonesia, Philippines), coupled with subduction slab-pull at the Java–Sunda–Sumatra trench, with associated subduction rollback and instability of the overthickened crust are the primary controlling mechanisms that drive (extensional) basin development in Sundaland, and especially Thailand (Morley *et al*. 2000, 2001, 2004; Watkinson *et al*. 2008; Tingay *et al*. 2010; Searle & Morley 2011; Pubellier & Morley 2014) (Figs 1 and 2b). Subduction of oceanic lithosphere at the Java–Sunda–Sumatra trench was initiated *c*. 45 Ma (Hall 2009). However, subduction initiation might be more diachronous than previously expected (Pubellier & Morley 2014). Following rifting in the Late Eocene–Oligocene, a drastic early Miocene change in stress orientation occurred (Pubellier & Morley 2014), and by the end of the early Miocene almost all of the Sundaland basins stopped rifting, except for basins associated with the South China Sea and the onshore Thailand basins (Pubellier & Morley 2014) as previously outlined. Extension during the Oligocene to Early Miocene in the Andaman Sea developed in an east–west direction (Srisuriyon & Morley 2014). Subsequently, the direction of extension changed to a NNW–SSE direction in the Early to early Middle Miocene, leading to a transtensional setting (Srisuriyon & Morley 2014).

The regional changes in stress orientation can be explained by a switch from subduction rollback and extensional collapse of the thickened lithosphere to transtension caused by the northward movement of India towards Eurasia, tectonic coupling between India and Myanmar and the Himalayan Orogeny (Morley 2017). However, the effects of stress changes are different in the Andaman Sea, Gulf of Thailand, and central and northern Thailand owing to their different locations with respect to the sources of stress.

Samples and methods

The samples analysed in this study originate from onshore eastern Thailand gneiss and granite outcrops, located on the northeastern margins of the Gulf of Thailand (Table 1 and Fig. 3). This area is intensively intersected by the fault networks related to the Mae Ping and Three Pagodas Fault zones (Figs 2b, 3 and 5). Using a small sampling resolution, samples were collected from several plutons belonging to different Thai granite provinces (e.g. Cobbing 1992) and therefore we could possibly evaluate potential differences in exhumation timing or exhumation rate along the different structural domains. Care was thus taken to sample several transects across the structural fabric and across known terrane boundaries. NT-01 and KM-01 are S-type granites from west of the Klaeng Fault line in the Main Range Central Granite Province of Thailand (Fig. 2a). KM-05 to KM-15 represent the Eastern Granite Province (I-type) (Fig. 2a). Other samples were taken from several metamorphic basement inliers, such as NT-02 and KM-04, which are from the metamorphosed rocks at Khao Chao along the Klaeng Fault zone, located between the Main Range and Eastern Granite Provinces (Figs 2a and 3). KM-04 originates from an area east of Rayong, and just north of Koh Samet, where paragneisses (Lem Khet Formation) from an Ordovican sedimentary protolith are exposed by low-angle normal faulting (Geard 2008; Morley *et al*. 2011). The migmatized granite sample KM-15 is the only sample located on the eastern side of the Sa Kaeo suture zone and is located on the main trace of the Mae Ping Fault (Figs 2b, 3 and 5).

Apatite fission-track dating

Apatite fission-track (AFT) dating is a low-temperature thermochronological method based on the spontaneous nuclear fission of ^{238}U, present as trace element in the crystal lattice of apatite. This fission process produces sub-microscopic linear radiation damage tracks (or fission tracks) in the apatite crystal lattice. These fission tracks are chemically etched with nitric acid to reveal the tracks for optical microscopic analysis at high magnification. At temperatures (T) lower than *c*. 60°C, natural fission tracks in apatite are considered stable and are retained on geological time scales, whereas at $T > \sim 120$°C the apatite crystal lattice regenerates and the fission tracks anneal rapidly (e.g. Wagner & Van den haute 1992; Ketcham *et al*. 1999; Donelick *et al*. 2005). The *c*. 60–120°C temperature window (corresponding to about 2–4 km crustal depth) represents the apatite partial annealing zone (APAZ) (Gleadow *et al*. 1986; Green *et al*. 1986). Here, tracks can accumulate but are progressively shortened, owing to partial annealing at the track ends. The apatite fission-track age, based on the measurement of the

Table 1. *Sample localities*

Sample	Latitude (N)	Longitude (E)	Altitude (m)	Lithology	Pluton	Analyses
NT-01	13°20′22.5″	100°55′28.8″	1	Biotite granite	Chonburi	AFT
NT-02	13°10′50.7″	101°24′17.0″	135	Gneiss	Ban Na Cham	AFT, AHe
KM-01	13°07.510′	101°05.238′	140	Biotite granite	Rayong	AFT
KM-04	12°38.485′	101°25.789′	28	Metagranite (foliated)	Ban Na Cham	AFT
KM-05	12°31.492′	102°10.652′	46	Granodiorite	Chantaburi	AFT
KM-06	12°32.635′	102°14.401′	51	Granite	Chantaburi	AFT
KM-07	12°45.868′	102°02.834′	40	Granodiorite	Khao Cha Mao	AFT, AHe
KM-08	12°52.919′	102°01.414′	57	Granite	Khao Cha Mao	AFT
KM-09	12°54.707′	101°43.120′	100	Granite (sheared)	Nong Yai	AFT, AHe
KM-10	13°00.515′	101°42.617′	87	Granite	Nong Yai	AFT
KM-11A	12°51.358′	102°06.658′	70	Granite	Klathing	AFT
KM-14A	13°01.321′	102°15.648′	177	Granite	Klathing	AFT
KM-14B	13°01.321′	102°15.648′	177	Granite	Klathing	AFT
KM-15	13°46.300′	102°00.518′	56	Migmatized granite	Sa Kaeo	AFT, AHe

Sample localities and lithology with indication of techniques used: apatite fission-track (AFT) and/or apatite (U–Th)/He (AHe).

etched areal spontaneous fission-track density, is a cooling age, and hence dates the time since fission tracks became thermally stable.

All samples in this study were analysed with the external detector (ED) method using thermal neutron irradiation, following the standard procedure from the AFT laboratory at Ghent University (e.g. De Grave & Van den haute 2002; De Grave *et al.* 2009, 2011; Glorie *et al.* 2010; Nachtergaele *et al.* 2018). Spontaneous fission tracks in apatite were etched in a 5.5M nitric acid solution for 20 s at 21°C. After irradiation, induced tracks were revealed in the muscovite ED (Goodfellow, clear ruby) with 40% hydrofluoric acid (HF) for 40 min at 21°C. Irradiation was carried out in the Belgian Reactor 1 (BR1) (De Grave *et al.* 2010). AFT ages are calculated using the overall mean weighted zeta based on Durango and Fish Canyon Tuff apatite age standards and IRMM 540 glass dosimeter, and are reported as conventional mean zeta-ages (t_ζ) (Hurford & Green 1983; Hurford 1990) as well as central ages (t_c) (Galbraith 1990; Vermeesch 2009). The AFT length distribution is used for time–temperature history reconstruction by inverse thermal history modelling (Ketcham *et al.* 1999, 2007*b*; Gallagher 2012). Where possible, 100 horizontal confined tracks per sample were measured at ×2000 magnification with a Nikon Eclipse Ni-E microscope equipped with a DS-Ri2 camera. For most of the

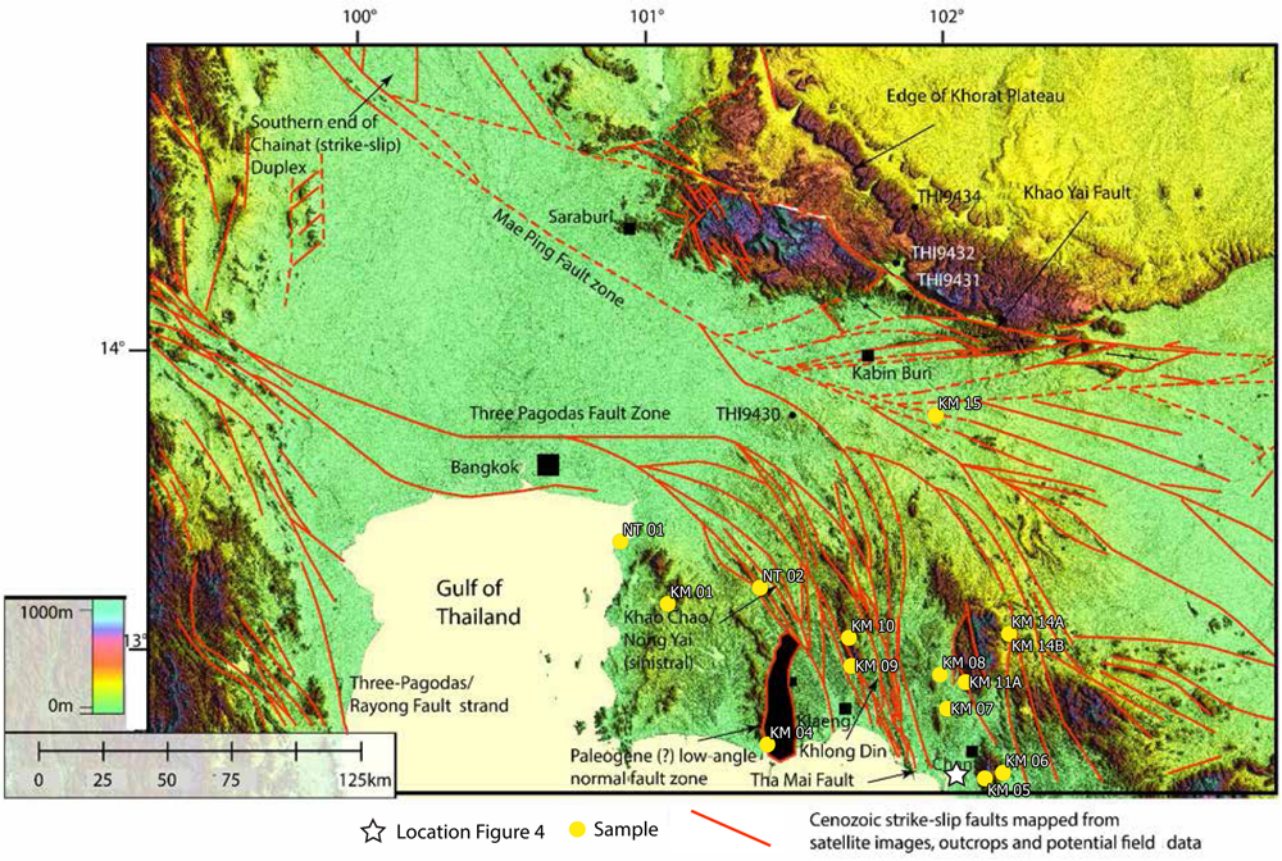

Fig. 3. Topographic map of southeastern Thailand with the analysed samples indicated by yellow dots. The few previously analysed samples of Upton (1999) (THI-numbers) close to the edge of the Khorat Plateau are also shown. Mapped Cenozoic strike-slip faults based on satellite images, outcrops and potential field data are illustrated with red lines.

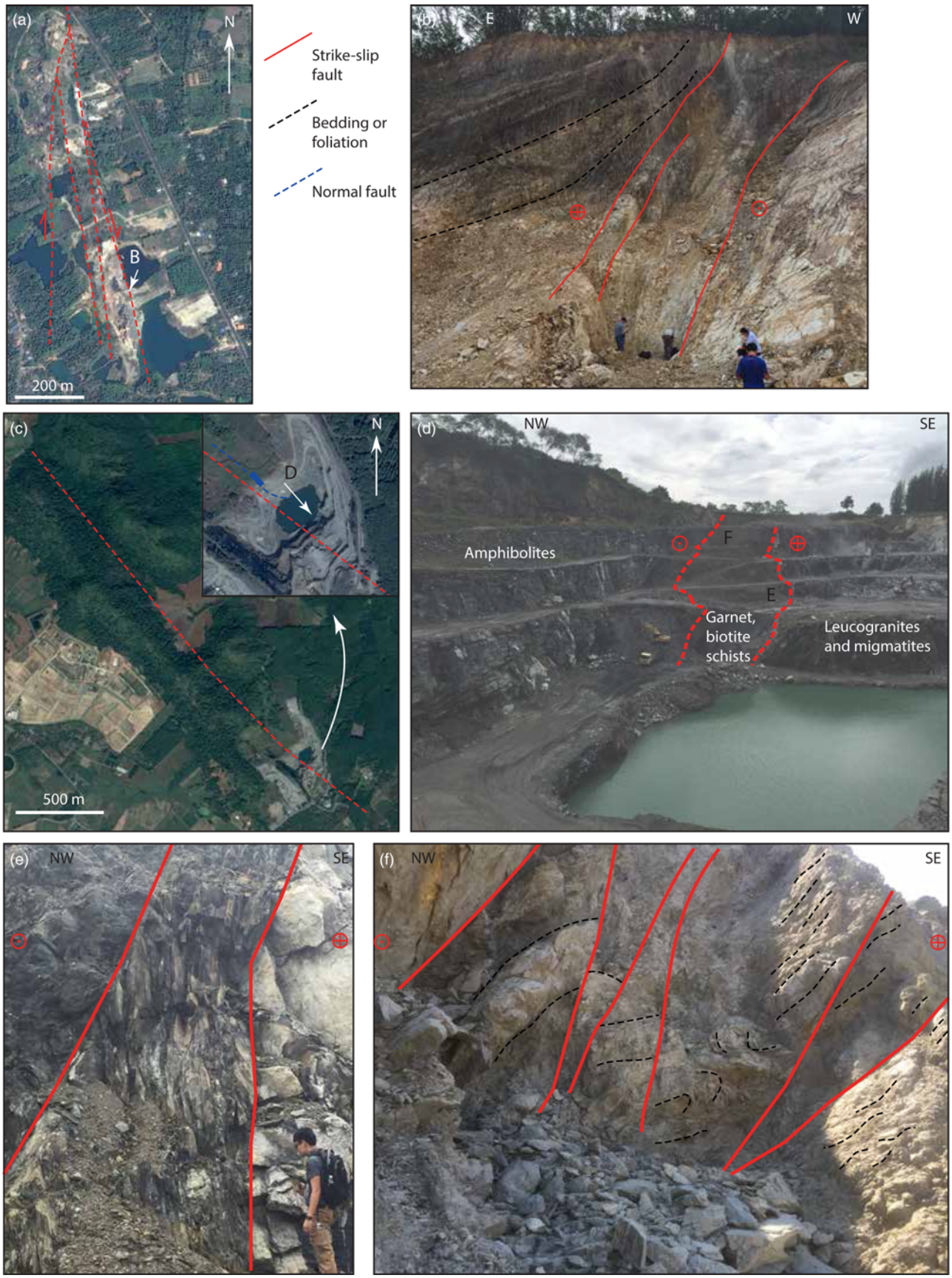

Fig. 4. Examples of strike-slip fault zones from the study area in outcrop. (**a**) Google Earth image (Map Data: CNES/Airbus Maxar Technologies) of NNW–SSE-trending strike-slip fault in Paleozoic sedimentary rocks south of Chantaburi, 12°31′47″N, 102°08′05″E. (**b**) Strike-slip fault in small quarry (see (**a**) for location). (**c**) Google Earth image (Map data: CNES/Airbus Maxar Technologies) of aggregate quarry in metamorphic rocks SW of Khao Chao, 13°13′56″N, 101°16′14″E. (**d**) View of quarry to SE showing the main lithologies cut by the brittle strike-slip fault (see (**c**) for location). (**e**) Splays of the strike-slip fault in garnet–biotite schist, juxtaposed with migmatites (see (**d**) for location). (**f**) Weathered part of strike-slip fault zone, showing internal folds and reverse faults (see (**d**) for location).

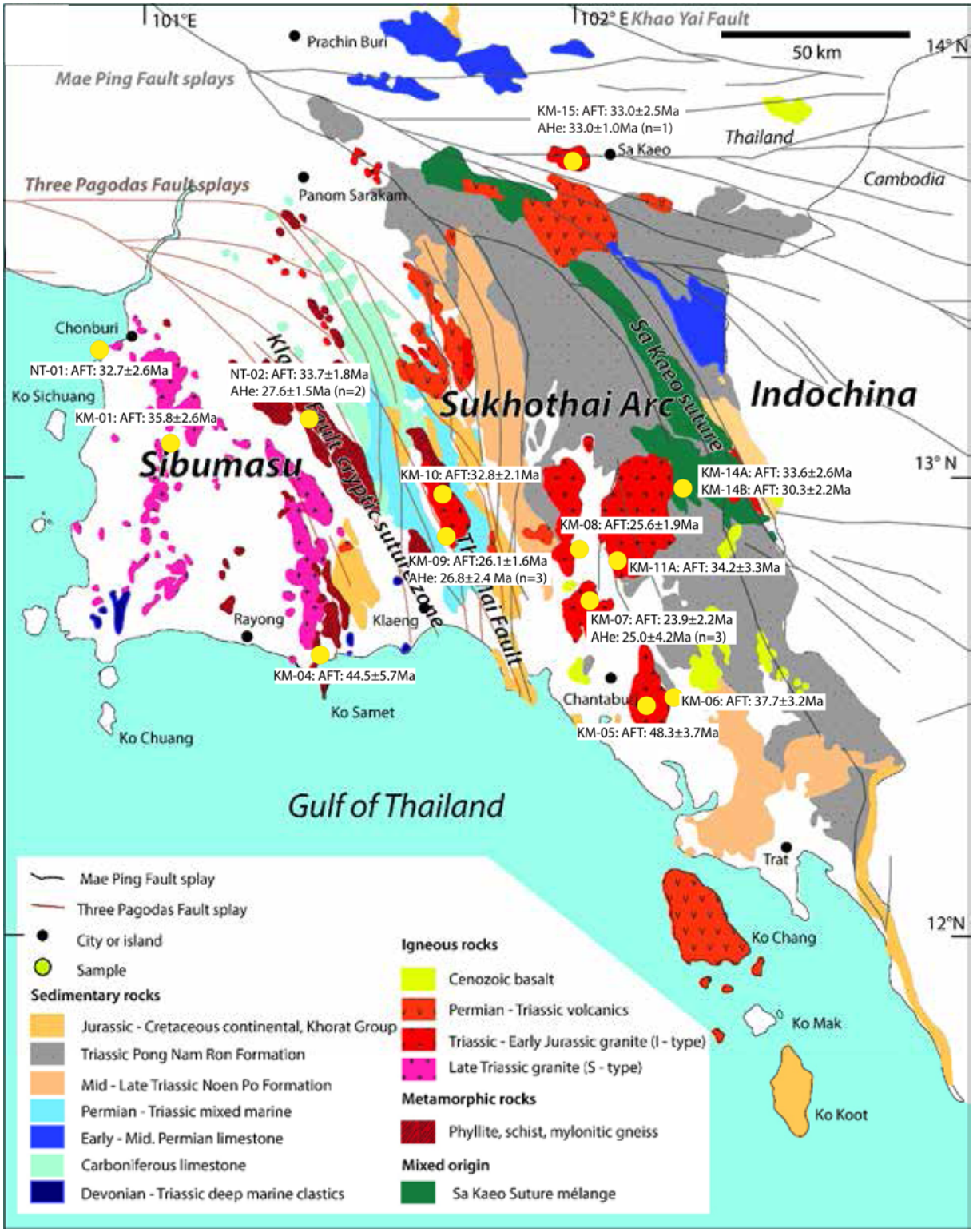

Fig. 5. Detailed geological map (based on Sone *et al*. (2012) and references therein) with sample locations and results of apatite fission-track (AFT) and apatite (U–Th)/He (AHe) dating. The brown lines indicate fault splays of the Three Pagodas Fault zone; the grey lines indicate fault splays from the Mae Ping Fault zone (based on Ridd & Morley 2011). (For location, see Fig. 2a and b.)

samples, limited length data were available owing to low spontaneous surface track densities and/or a low number of suitable grains. Hence, duplicate apatite mounts were made for ^{252}Cf irradiation to enhance the number of confined tracks (Donelick & Miller 1991). Thermal history modelling was performed for NT-02 and KM-14B using the QTQt software (Gallagher 2012), with *c*-axis projection (Ketcham *et al*. 2007*a*) and using the Ketcham *et al*. (2007*b*) annealing equations and the Markov Chain Monte Carlo search method for inverse modelling. Both samples (NT-02 and KM-14B) have enough track lengths (±100) so that the uncertainty for both thermal history models should be rather low (Barbarand *et al*. 2003). For samples with 40–100 track lengths, a thermal history has been reconstructed and can be found in supplementary material, appendix 5. During thermal history modelling, it was not possible to choose the appropriate geometry for each apatite crystal that was analysed during apatite (U–Th)/He analysis, because it is

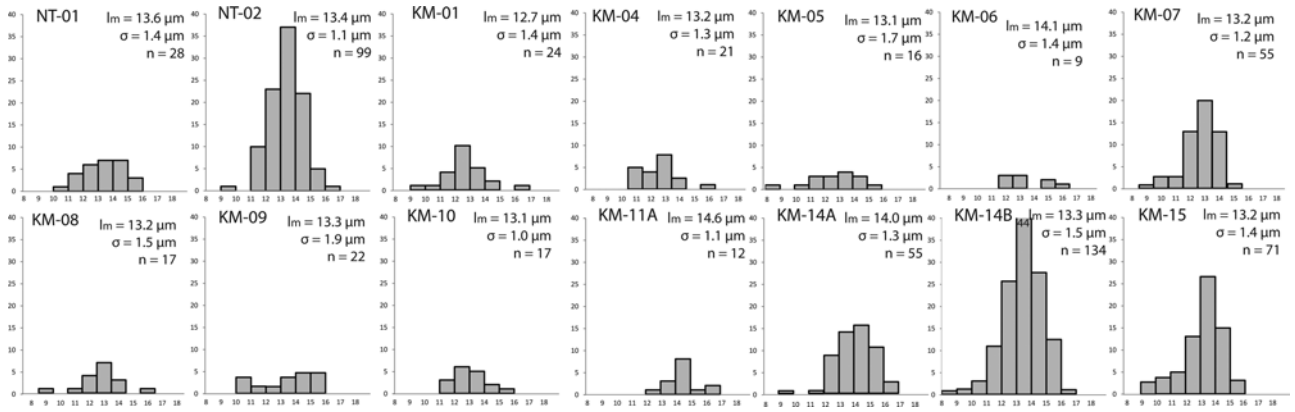

Fig. 6. Confined fission-track length histograms of the analysed samples (for locations, see Fig. 3). The number of measured confined tracks and the length (in µm) is indicated on the vertical and horizontal axis, respectively. Mean track lengths (l_m), standard deviation (σ) and number of tracks (n) are displayed. Most confined track length data consist of <40 confined track length measurements, owing to a low density of spontaneous tracks in the etched apatite grains. Hence, Cf-irradiation was performed on separate mounts for samples KM-04, KM-07, KM-09, KM-14A, KM-14B and KM-15 and subsequent measurement results were added. Some samples with sufficient length measurements (>100) will be used for thermal history modelling in Figure 7, following the recommendations of Barbarand *et al*. (2003). Samples with >40 length measurements were modelled and can be found in supplementary material, Appendix 5.

only possible to choose the sphere (2T), infinite slab, infinite cylinders and hexagonal fragments (1T) in QTQt (v5.6.0). Erroneous F_T correction can lead to wrong corrected AHe ages and therefore we chose not to incorporate the apatite (U–Th)/He data in the thermal history model. The presented AFT data have been added as supplementary material, Appendix 2 and the detailed procedure of thermal history modelling has been described in supplementary material, Appendix 4, which incorporates all necessary information in a standard format as proposed by various researchers (Flowers *et al*. 2015; Gallagher 2016).

Apatite (U–Th)/He dating

Apatite (U–Th)/He (AHe) dating is also a low-temperature dating technique and is based on the production (and diffusion and implantation) of α-particles (^{4}He nuclei) produced in the α-decay reaction series from ^{238}U, ^{235}U and ^{232}Th, and to a lesser extent ^{147}Sm, to their respective stable radiogenic daughters (^{206}Pb, ^{207}Pb and ^{208}Pb respectively, and ^{143}Nd for ^{147}Sm) (Zeitler *et al*. 1987). The AHe dating technique has a presumed closure temperature of about *c*. 70°C for cooling rates of 10°C Ma^{-1} (Ehlers & Farley 2003) and in that sense is therefore complementary to the AFT method. An F_T correction factor for each isotope (^{238}U, ^{235}U and ^{232}Th) based on the geometry of the analysed apatite crystal is critical to correct the individual age for α-particle diffusion through the crystal lattice (Ketcham *et al*. 2011; Table 2). The geometry can be cylindrical, hexagonal without pyramidal terminations (0T), with one pyramidal termination (1T) or with two pyramidal terminations (2T) (see Ketcham *et al*. 2011).

AHe analyses were performed in the London Geochronology Centre of University College London. ^{4}He measurements were made with the Pfeiffer Prisma 100 quadrupole mass spectrometry system using a ^{3}He spike. Apatite grains encased in platinum crucibles were heated *in vacuo* to *c*. 850°C using an infrared laser system for 120 s, with a degassing time of 300 s, and subsequently retrieved from the vacuum system. A secondary reheating and measuring step was applied for each aliquot, to detect possible incomplete degassing owing to, for example, mineral inclusions. Following helium extraction the chamber was opened and aliquots were removed from the Cu planchet and placed into Teflon beakers. Subsequently the aliquots were dissolved in HNO_3, spiked with ^{230}Th and ^{235}U, and analysed for U and Th isotopes by inductively coupled plasma mass spectrometry (ICP-MS) with an Agilent 7700x system. A blank vial of the HNO_3 digestive solution and vials of a U standard with known ^{238}U concentration were added to the ICP-MS run so that sample measurements could be calibrated. Reported He ages were corrected for α-ejection effects based on measured grain dimensions using the procedure of Ketcham *et al*. (2011). Each sample typically comprised four aliquots. Data reduction, error propagation and central age calculation were performed with HelioCalc (https://www.ucl.ac.uk/~ucfbpve/heliocalc/). More detailed information on the analytical procedures can be found in text appendix S1 of Wildman *et al*. (2017).

Results

Apatite fission-track data

All our obtained apatite fission-track (AFT) ages are Cenozoic and range from 48 to 23 Ma (Table 3, Figure 5), with the majority of central ages concentrated near the Eocene–Oligocene transition around *c*. 33 Ma. Spontaneous track densities are low for almost all of the samples, owing to a combination of the relatively young AFT ages and low U concentrations of the apatite grains (Table 3). Consequently, only around 20 confined tracks were found in most of the samples, producing only limited information on the track length distributions. For some samples, ^{252}Cf bombardment increased the number of measurable, horizontal fission tracks and these samples are indicated with an asterisk in Table 3. However, for sample NT-02 a total of 99 confined track lengths were measured, yielding a unimodal distribution with mean track length of 13.4 µm (Fig. 6). For KM-14B, the mean track length, based on 134 lengths, is 13.3 µm but is slightly more negatively skewed than that for NT-02. The other samples show a small number of track lengths, but roughly confirm the observations from both previous samples, with mean track lengths that range from 12.7 to 14.6 µm and standard deviations ranging from 0.9 to 1.9 µm. Generally, all length histograms have unimodal distributions with relatively long mean track lengths around 13–14 µm, in a few cases subtle negatively skewed, and can be considered as typical for rapidly cooled basement samples (Fig. 6) (Gleadow *et al*. 1986). All samples pass the $P(\chi^2)$ homogeneity test, except for KM-01, KM-04 and KM-11A (Table 3). Radial plots with D_{par} measurements can be consulted in supplementary material, Appendix 3 of this paper. The kinetic parameter D_{par} ranges from 1.12 to 1.83 µm for our samples, which is indicative of chlorine-poor apatite (Donelick 1993) that

Table 2. *Apatite (U-Th)/He crystal dimensions*

Sample	Geometry	Height (μm)	Width (μm)	Thickness (μm)
NT-02 (3)	Cylindrical	163.2	86.9	83.4
NT-02 (4)	Hexagon 1T	252.0	227.0	186.1
KM-07 (1)	Hexagon 2T	142.1	114.9	96.6
KM-07 (2)	Hexagon 0T	196.3	76.15	74.4
KM-07 (3)	Hexagon 2T	158.6	116.9	107.9
KM-07 (4)	Hexagon 1T	109.4	76.2	71.7
KM-09 (1)	Hexagon 2T	108.4	80.0	68.6
KM-09 (2)	Hexagon 1T	193.0	88.4	72.9
KM-09 (3)	Hexagon 0T	166.0	76.0	72.0
KM-09 (4)	Cylindrical	182.9	66.8	63.1
KM-15 (1)	Hexagon 2T	244.2	100.3	89.0
KM-15 (2)	Hexagon 2T	157.7	75.4	66.9
KM-15 (3)	Hexagon 2T	132.7	67.3	68.2
KM-15 (4)	Hexagon 0T	193.2	99.0	82.3

This geometry and exact dimensions are shown here for all analysed apatite crystals during apatite (U–Th)/He analysis.

characteristically exhibits more rapid annealing of latent fission tracks (Green *et al*. 1986).

Apatite (U–Th)/He data

Four samples were prepared for apatite (U–Th)/He (AHe) dating. They all generally contain U-poor apatite grains (Table 4). F_T correction factors for ^{238}U, ^{235}U and ^{232}Th and F_T corrected ages were calculated with the HelioCalc software (Vermeesch; http://www.ucl.ac.uk/~ucfbpve/heliocalc/) based on each separate geometry (e.g. hexagonal 0T, hexagonal 1T, hexagonal 2T or cylindrical) of each analysed apatite crystal. Subsequently, some grains that degassed incompletely during laser fusion were discarded for further calculations (Table 4). Although an absolute minimum of apatite grains were analysed for each sample, consistent and reproducible ages were obtained, and a mean weighted AHe age was calculated for each of the samples. These weighted mean ages scatter between 33 and 25 Ma (Table 4). AHe mean weighted ages are within one standard error of their corresponding AFT central ages and are generally somewhat younger than the AFT age. Weighted mean age calculation was not possible for KM-15 because of significant outliers or incomplete degassing (Table 4). Only a single aliquot age of about 33.0 ± 1.0 Ma could thus be retained for this sample. Aliquot NT-02 (2) was not measured owing to a technical problem during analysis. Over-dispersed AHe ages (such as for KM-15) can be the result of several processes, such as the presence of U-rich inclusions (Stockli *et al*. 2000). Many fundamental questions concerning this over-dispersion still remain to be solved (Green & Duddy 2018; Van Ranst *et al*. 2019).

Thermal history modelling

The thermal history model for sample NT-02, based on its AFT age and length data ($n = 99$), is well constrained and indicates a two-stage thermal history. A rapid cooling phase is predicted to last until about 33 Ma, when slow cooling eventually brings the samples to ambient present-day surface temperatures. The mean weighted AHe age of 27.6 ± 1.5 Ma for NT-02 is in excellent agreement with the thermal history model of NT-02, if we assume an AHe closure temperature of *c.* 60–75°C. Moderate cooling, thus slower than for NT-02, is observed for KM-14B between 40 and 20 Ma (Fig. 7). Considering the relatively long mean track lengths of >13 μm in all samples (Fig. 7), except KM-01, and the occurrence of the 40–30 Ma cooling path in both reconstructed thermal history models, a late Eocene–earliest Oligocene rapid cooling event is clearly expressed in the data. The rapid cooling between 30 and 23 Ma could not be illustrated with thermal history models because of the low number of confined track length measurements, but thermal history models of these samples have been constructed and can be consulted in supplementary material, Appendix 5.

Discussion

Cenozoic exhumation–denudation history of Thailand

Low-temperature thermochronometry techniques such as AFT and AHe dating were applied on basement rocks originating from the Central and Eastern Granite Provinces. All AFT and AHe central ages are Eocene–Oligocene and range from 48 to 24 Ma, with most of the AFT and AHe ages concentrated around 36–24 Ma (late Eocene–Oligocene). Our data are in agreement with scarce existing low-temperature thermochronological data obtained on basement or sedimentary rocks in Thailand, which can be consulted in supplementary material, Appendix 1 (Putthapiban 1984; Racey *et al*. 1997; Upton 1999; Morley *et al*. 2007). For example, an AFT age of 31 ± 3 Ma was obtained on granitic basement (THI9430) in the NW of our study area (Upton 1999) (Fig. 3). Our results are also comparable with unpublished AFT data of S. Meffre (reported by Morley *et al*. 2011) that indicate basement cooling from 38 to 22 Ma obtained from three granite samples in the Rayong fault zone area. Localized metamorphism in the Klaeng Fault strike-slip zone is constrained by monazite U–Pb ages of 42.54 ± 0.88 Ma and 35.5 ± 3.1 to 37.8 ± 4.8 Ma for titanite U–Pb (Geard 2008) and suggests a much later (Eocene) metamorphic overprint than previously suggested (Kawakami *et al*. 2014). Based on NW–SE shearing indicators and additional zircon U–Pb dating on deformed basement rocks exposed in this area, ductile sinistral shearing of the Klaeng Fault zone has been shown to have occurred after 67 ± 1 Ma (Kanjanapayont *et al*. 2013). Also, based on the unpublished monazite and titanite U–Pb ages of Geard (2008), an Eocene age for the NW–SE-directed sinistral shearing was assumed. Our low-temperature thermochronometric data suggest that during this Eocene shearing, coeval basement exhumation brought the investigated rocks to upper crustal levels. Some of the AFT (KM-07, KM-08, KM-09) and AHe samples (KM-07, KM-09) suggest a latest phase of rock cooling during the Oligocene (Tables 3 and 4; Fig. 8; supplementary material, Appendix 5). At this time paleostress indicators show that shear senses shifted to dextral (Lacassin *et al*. 1997).

Sample NT-02 from within the Klaeng Fault zone yields a thermal history model exhibiting cooling before 33 Ma (Fig. 7). The AFT central age for sample NT-02 of 33.7 ± 1.8 Ma combined with a unimodal, moderate to high mean track length value of 13.4 μm and two single grain AHe (F_T-corrected) ages of 25.4 ± 0.5 and 29.7 ± 0.3 Ma indicate rapid cooling and associated final late Eocene–early Oligocene exhumation to shallow crustal levels of the metamorphosed rocks exposed in the Klaeng Fault zone (Khao Chao area). This hence immediately follows peak metamorphic conditions (Geard 2008). The migmatized granite KM-15, which is located on the main fault trace of the Mae Ping Fault system in the area, has an AFT age of 33.0 ± 2.5 Ma, with a mean track length of 13.2 μm (based on 71 length measurements), and one AHe aliquot with an age of 33.1 ± 1.1 Ma, and provided one retained, albeit incompletely degassed aliquot of 26.6 ± 3.6 Ma. This indicates fast cooling along the Mae Ping Fault zone around the Eocene–Oligocene transition and is in accordance with $^{40}Ar/^{39}Ar$ cooling ages from micas associated with the last phase of sinistral movement on the Three Pagodas Fault (36–33 Ma) further afield and the Mae Ping Fault zone (33–30 Ma) in western Thailand (Lacassin *et al*. 1997; Nantasin *et al*. 2012). The opening of the Cuu Long basin in south Vietnam (i.e. SE of our study area) is also considered a direct

Table 3. *Apatite fission-track (AFT) data*

Sample	n	ρ_s (±1σ)	N_s	ρ_i (±1σ)	N_i	[U]	ρ_d (±1σ)	N_d	ρ_s/ρ_i (±1σ)	$P(\chi^2)$	Disp.	t_ζ	t_c	l_m	n_l	1σ	D_{par}
NT-01	25	4.772 (0.226)	262	9.594 (0.409)	551	25.2	4.822 (0.098)	2411	0.508 (0.038)	0.96	0.0036	35.0 ± 2.8	32.7 ± 2.6	13.6	28	1.4	1.37
NT-02	20	8.302 (0.320)	672	16.836 (0.320)	1373	44.2	4.822 (0.098)	2411	0.520 (0.024)	0.40	0.52	35.8 ± 1.9	33.7 ± 1.8	13.4	99	1.1	1.23
KM-01	23	9.538 (0.399)	571	18.548 (0.550)	1138	46.9	5.017 (0.100)	2508	0.533 (0.027)	0.03	19.6	38.2 ± 2.2	35.8 ± 2.6	12.7	24	1.4	1.20
KM-04*	23	2.641 (0.150)	271	4.901 (0.213)	532	12.0	5.169 (0.102)	2581	0.749 (0.056)	0.00	45.4	*55.1 ± 4.2*	*44.5 ± 5.7*	13.2	21	1.3	1.12
KM-05	20	4.570 (0.254)	325	6.718 (0.301)	496	17.5	5.026 (0.100)	2513	0.643 (0.046)	0.65	2.43	46.1 ± 3.5	48.3 ± 3.7	13.1	16	1.7	1.17
KM-06	19	2.361 (0.154)	234	2.361 (0.154)	458	11.2	5.168 (0.102)	2584	0.541 (0.043)	0.40	1.35	39.9 ± 3.3	37.7 ± 3.2	14.1	9	1.4	1.24
KM-07*	20	2.754 (0.169)	265	8.667 (0.302)	822	21.2	5.174 (0.102)	2587	0.336 (0.024)	0.24	19.6	24.8 ± 1.8	23.9 ± 2.2	13.2	55	1.2	1.28
KM-08	25	3.040 (0.177)	296	8.655 (0.296)	853	21.2	5.180 (0.102)	2590	0.363 (0.024)	0.89	3.6	26.8 ± 1.9	25.6 ± 1.9	13.2	17	1.5	1.23
KM-09*	25	1.196 (0.097)	150	3.302 (0.160)	425	8.1	5.188 (0.102)	2594	0.401 (0.038)	0.79	0.097	29.7 ± 2.9	26.1 ± 2.6	13.3	22	1.9	1.33
KM-10	29	3.368 (0.165)	415	7.507 (0.246)	934	18.9	5.030 (0.100)	2515	0.464 (0.027)	0.85	5.40	33.3 ± 2.1	31.9 ± 2.1	13.1	17	1.0	1.13
KM-11A	10	11.484 (0.578)	395	24.249 (0.834)	846	59.2	5.194 (0.102)	2597	0.490 (0.030)	0.03	18.5	36.3 ± 2.3	34.2 ± 3.3	14.6	12	1.1	1.55
KM-14A*	20	2.999 (0.182)	271	6.569 (0.269)	297	16.0	5.206 (0.102)	2603	0.481 (0.035)	0.35	3.76	35.8 ± 2.7	33.6 ± 2.6	14.0	55	1.3	1.81
KM-14B*	20	3.630 (0.177)	422	8.767 (0.271)	1044	21.3	5.212 (0.102)	2606	0.433 (0.025)	0.08	15.8	32.2 ± 1.9	30.3 ± 2.2	13.3	134	1.5	1.83
KM-15*	25	3.111 (0.187)	278	6.283 (0.251)	627	15.3	5.218 (0.102)	2609	0.511 (0.037)	0.73	0.92	38.0 ± 2.8	33.0 ± 2.5	13.2	71	1.4	1.38

Apatite fission-track data of basement apatites from southeastern Thailand: n grains were analysed for each sample. ρ_s and ρ_i represent the areal density of the etched spontaneous and induced fission tracks (measured in the external detector) respectively. N_s and N_i correspond to the number of counted spontaneous and induced fission tracks. [U] indicates the mean uranium concentration of the analysed grains using the appropriate formula (Enkelmann *et al.* 2005). ρ_d values are linearly interpolated values of the track density in the external detector attached to the uranium-doped glass dosimeters (IRMM-540; De Corte *et al.* 1998). ρ_s, ρ_i and ρ_d values are expressed as 10^5 tracks cm^{-2}. $P(\chi^2)$ represents the chi-squared probability that the ρ_s/ρ_i ratio is constant. The degree of dispersion is also shown. Zeta t_ζ and central ages t_c are given for each sample (in Ma). The mean track lengths (l_m) are based on limited numbers (n_l) of confined track length measurements. The standard deviation on the confined track length distribution (σ) and the etch pit diameter (D_{par}) is also reported. All samples were analysed by S. Nachtergaele, who has a personal zeta-factor of 286.2 ± 4.7 a cm^2 calibrated on multiple Durango and Fish Canyon Tuff age standards and the IRMM-540 glass (De Corte *et al.* 1998).
*Samples benefited from ^{252}Cf irradiation to increase the number of confined track length measurements.

Table 4. *Apatite (U–Th)/He data*

Sample	Geometry	U (ppm)	σ	Th (ppm)	σ	He (pmol)	He error (%)	eU	σ	F_T (^{238}U)	F_T (^{235}U)	F_T (^{232}Th)	Uncorr. age (Ma)	σ	Corr. age (Ma)	σ	Weighted mean age (1σ; n)
NT-02 (3)	Cylindrical	40.205	0.432	9.23	0.1	0.01301	0.00023	42.37	0.433	0.757	0.721	0.715	19.144	0.398	25.4	0.527	27.6 Ma (1.5 Ma; 2)
NT-02 (4)	Hexagon 1T	21.04	0.224	2.655	0.027	0.058	0.00015	21.66	0.224	0.863	0.842	0.839	25.614	0.272	29.7	0.316	
KM-07 (1)	Hexagon 2T	69.396	0.625	137.5318	0.9788	0.0123	0.00022	101.7	0.666	0.731	0.69	0.684	10.889	0.212	15.2	0.297	25.02 Ma (4.19 Ma; 3)
KM-07 (2)	Hexagon 0T	22.925	0.328	72.441	0.778	0.01215	0.00023	39.94	0.376	0.698	0.654	0.648	22.01	0.467	32.6	0.693	
KM-07 (3)	Hexagon 2T	37.596	0.382	87.546	0.667	0.01689	0.00024	58.17	0.413	0.751	0.713	0.708	20.248	0.32	27.6	0.436	
KM-07 (4)	Hexagon 1T	19.46	0.428	75.268	0.839	0.00543	0.00022	37.14	0.471	0.656	0.607	0.599	24.44	1.03	38.9	1.64	
KM-09 (1)*	Hexagon 2T	1.15	0.3	26.925	0.294	0.00086	0.00021	7.48	0.3	0.64	0.588	0.58	25.61	6.31	43	11	26.8 Ma (2.4 Ma; 3)
KM-09 (2)	Hexagon 1T	1.82	0.13	13.22	0.117	0.00133	0.00021	4.92	0.13	0.718	0.676	0.67	18.88	3.09	27.5	4.5	
KM-09 (3)	Hexagon 0T	1.66	0.12	18.817	0.182	0.00104	0.00021	6.09	0.13	0.689	0.644	0.637	14.86	3.1	22.8	4.76	
KM-09 (4)	Cylindrical	4.38	0.2	17.658	0.18	0.00176	0.00021	8.53	0.2	0.705	0.661	0.655	19.63	2.44	28.9	3.6	
KM-15 (1)*	Hexagon 2T	33.461	0.343	142.007	1.118	0.1905	0.0014	66.83	0.347	0.757	0.721	0.715	132.543	1.271	179.6	1.723	Single grain age: 33.0 ± 1.0 Ma
KM-15 (2)	Hexagon 2T	25.372	0.391	83.933	0.711	0.00713	0.00022	45.09	0.324	0.672	0.624	0.617	21.398	0.695	33.1	1.07	
KM-15 (3)*	Hexagon 2T	16.602	0.407	27.806	0.3	0.00196	0.00026	23.13	0.304	0.639	0.586	0.578	16.52	2.24	26.6	3.61	
KM-15 (4)*	Hexagon 0T	74.18	4.96	373	19	0.01185	0.00023	161.8	6.797	0.744	0.707	0.701	3.53	0.16	4.9	0.23	

The concentrations and analytical uncertainty of the U, Th and He measurements are displayed for each aliquot. Uncorrected ages are subsequently corrected for He ejection based on the geometry and specific dimensions of the analysed apatite crystal. Mean ages are calculated with IsoplotR (Vermeesch 2018).
*Incomplete degassed grains (e.g. KM-09 (1) and KM-15 (3)) and grains with anomalous ages (KM-15 (1), KM-15 (4)) were not used in this calculation.

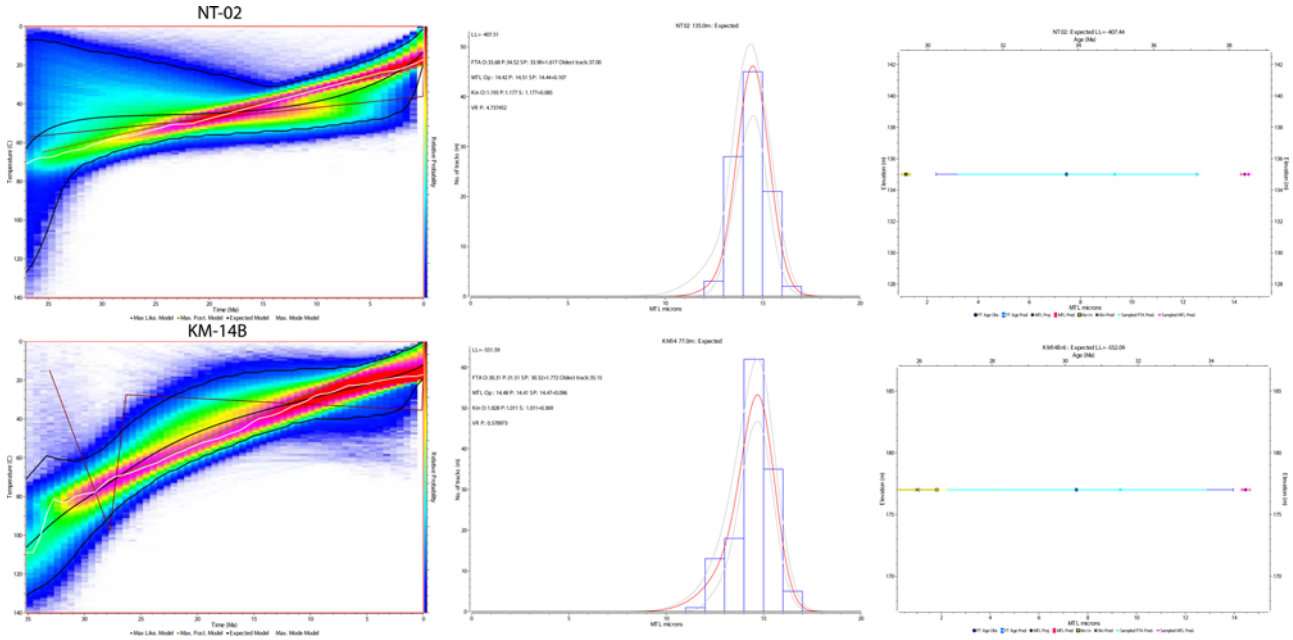

Fig. 7. Time–temperature reconstructions or thermal history models (left) for NT-02 (upper) and KM-14B (lower), reconstructed with the QTQt modelling software (Gallagher 2012). The colour-scale indicates relative probability for residence at that particular time–temperature point in geological time. The input parameters from the confined track length measurements and fit of the most likely model are given in the middle panel. The predicted and observed values for the kinetic parameter, apatite fission-track age and mean track length are shown in the right panel.

consequence of sinistral fault activity of the Mae Ping Fault zone from 40 to 31 Ma (Schmidt *et al*. 2019). Here also, a marked change to a dextral shear sense around 31–25 Ma is registered. The low-*T* thermochronological data presented in this paper therefore connect the two study areas (western Thailand and south Vietnam) and are in agreement with both proposed tectonic models.

The thermal history models presented here visualize how cooling of the basement rocks to shallower depths transpired. On the one hand, exhumation could be tectonic, as is the case, for example, for basement rocks located in the hanging wall of low-angle faults controlling the opening of sedimentary basins. For example, KM-04 is located in the hanging wall of an east-dipping low-angle normal fault, identified by Geard (2008). Hence, the AFT age could represent the age of tectonic exhumation. On the other hand, AFT ages can also constrain the timing of erosional removal of the exhumed basement blocks. These basement blocks consequently provide source material for the developing adjacent basins. Indeed, coarse conglomerates and breccias overlain by fluvial sandstones and fluvial and fluvial–deltaic mudstones are the typical sequence at the base of an offshore rift basin of the Gulf of Thailand (Morley & Racey 2011). These coarse-grained deposits are interpreted as local erosion products originating from removal of rock-burden of uplifted areas. The cause of rapid exhumation along the strike-slip fault zones is probably related to erosion during thickening and uplift in positive flower structures. Alternatively, the gravitational collapse that triggered extension in the Gulf of Thailand could have promoted a change from transpression to transtension along the strike-slip faults as well. In support of this model, extensional faults parallel to the strike of strike-slip faults in gneiss terrains are known from both the Mae Ping Fault zone in the Lansang national park (Lacassin *et al*. 1997) and from the Khao Chao area (Fig. 4a).

KM-14B lies west of the main Mae Ping Fault zone network, and east of the Three Pagodas Fault zone network. Denudation and its associated basement cooling occurred between 32 Ma and present time, and has a slightly slower rate than for the previous sample (Fig. 7). Strike-slip deformation in the region is very diffuse (Fig. 3), hence the effects are likely to be a more gradual regional exhumation over a broad area, rather than focused exhumation along a specific narrow strike-slip fault zone (in contrast to sample NT-02).

The late Oligocene AFT ages of KM-07 (23.9 ± 2.2 Ma), KM-08 (25.7 ± 1.9 Ma) and KM-09 (25.3 ± 2.5 Ma) and AHe ages for KM-07 (weighted mean 25.0 ± 4.2 Ma) and KM-09 (weighted mean 26.8 ± 2.4 Ma) obtained on the exposed plutons north of Chantaburi town could indicate continued cooling in the late Oligocene through movement along the Tha Mai Fault (Fig. 5). The Tha Mai Fault zone lies in the region of overlap between the branches of the Three Pagodas and the Mae Ping Fault zones (Ridd & Morley 2011) (Fig. 5). Here, it might be the case that a phase of dextral movement along the Mae Ping and Three Pagodas Fault zones exerts its influence on basement cooling. This has also been observed in the Chainat Duplex (Fig. 2), where it is estimated that dextral motion along the Mae Ping Fault took place with comparable late Oligocene–Miocene timing (Smith *et al*. 2007). Further SE in south Vietnam, dextral lateral motion estimated from 31 to 25 Ma along the Mae Ping Fault was responsible for a phase of compression in the Cuu Long basin (Schmidt *et al*. 2019).

The oldest AFT central ages found in the collected low-temperature thermochronological dataset of samples KM-04 (45.5 ± 5.7 Ma) and KM-05 (48.3 ± 3.7 Ma) hint that there might be a south to north younging trend, and it should be noted that both of them lie closest to the coast. This coincidence might suggest that the coastal region was exhumed first, and was also first to cease exhuming, followed by inland sites, which would fit with a rifting–thermal subsidence model, with the region of rifting located to the south. Admittedly, although our results hint at this possibility, more data should be collected to verify this model further. Another hypothesis to explain the 'old' AFT ages in the southern coastal region is that the fault network of the Mae Ping and Three Pagodas Fault zones had little influence during the Oligocene on the uplift history of KM-04 and KM-05. Perhaps these granitic plutons were exhumed earlier during a late Cretaceous–Paleocene event, which is now largely overprinted through later exhumation–denudation pulses in the Eocene–Oligocene. Low-temperature thermochronological data confirm that this event caused basement cooling in Cambodia in the Kampot Fold Belt (Fyhn *et al*. 2016). More

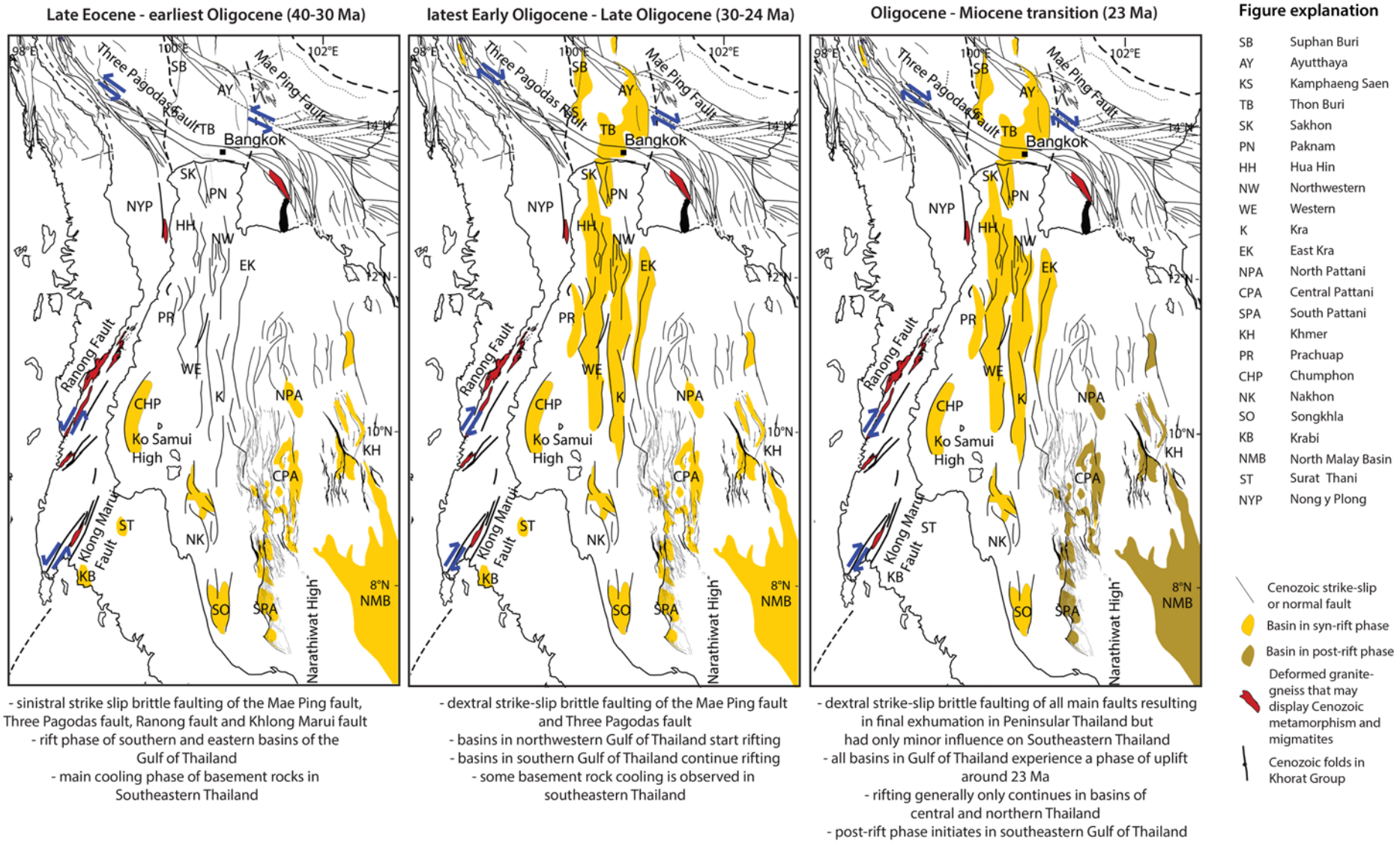

Fig. 8. Evolution of the intracratonic basins and major fault zones of southern Thailand, adapted from Morley (2015). The blue arrows indicate the sense of strike-slip movement of the major strike-slip faults. All information below the figures is extracted from the literature. Sources were cited in the geological setting section of this paper.

geochronological evidence indicates metamorphism in this area during the Late Cretaceous–Paleocene–Eocene. This includes, for example, the zircon U–Pb ages from Kanjanapayont *et al.* (2013) as young as 67 ± 1 Ma and monazite U–Pb ages of 43 ± 1 Ma from Geard (2008) from the Khao Chao gneisses, and zircon U–Pb ages of 49.6 ± 0.9 to 47.2 ± 1.4 Ma from the Khao Chamao (15 km east of the Khao Chao gneisses; i.e. KM-09 and KM-10) (Geard 2008).

Further south of our study area in the eastern Gulf of Thailand, rifting ceased around 23 Ma in the Pattani, Khmer and Northern Malay basin (Morley 2015) (Fig. 2b). In the western Gulf of Thailand, an episode of basin inversion occurred in the Chumphon basin around 23 Ma and can be connected to cooling of granites and gneisses along the Ranong Fault (Upton 1999). A recent report of the Department of Mineral Fuels, Ministry of Energy (2018) based on unpublished data indicated a phase of inversion at *c.* 23 Ma (and in some cases even erosion) in all large basins of the Gulf of Thailand (Pattani, Northern Malay, Khmer, Songkhla, Chumphon, Kra, Western basin). The cessation of rifting and subsequent onset of thermal subsidence in the eastern Gulf of Thailand ranges between about 23 and 10 Ma in the NW; consequently, such a diachronous event is unlikely to be represented by simple cooling age patterns onshore. However, overall the Late Eocene to late Oligocene low-*T* thermochronological ages overlap with the timing of opening of the basins offshore and the phase of uplift at *c.* 23 Ma in the eastern Gulf of Thailand (Fig. 8). After 23 Ma, when rifting ceased in the eastern Gulf of Thailand, little onshore exhumation occurred in southeastern Thailand.

In a broader context, the northern Mergui and northern Sumatra basins (Fig. 2b) ceased rifting around the late Oligocene–Early Miocene transition (*c.* 23 Ma) (Morley 2017). The drastic stress change in Sundaland as a whole in the early Miocene is explained by cessation of sea-floor spreading in the South China Sea and the end of subduction rollback in the Java–Sunda–Sumatra trench (Pubellier & Morley 2014). In the early Miocene, there was a switch from subduction rollback and extensional collapse of the thickened lithosphere of Thailand to transtension, caused by the northward migration of India towards Eurasia and tectonic coupling between India and Myanmar (Morley 2017). Dextral motion along the Sagaing Fault (Myanmar) since the late Oligocene (28–27 Ma) (Morley & Arboit 2019) is a direct consequence of the tectonic coupling between India and Myanmar. Our new late Eocene to late Oligocene low-temperature thermochronological data fit in this overall regional geodynamical picture, characterized by the opening of several on- and offshore basins and hence the contemporaneous cooling of the adjoining basement rocks, which is illustrated in Figs 7 and 8.

Importance of inherited structures

The north–south alignment of the sedimentary basins and strike direction of the associated faults is controlled by zones of crustal weakness inherited from the Indosinian Orogeny (Morley *et al.* 2004, 2011). The recent hypothesis on continental rifting initiation indicates the requirement of pre-existing linear weaknesses and rotational extension (Molnar *et al.* 2018). The first requirement is fulfilled, as the majority of the intracontinental rift basins of the Gulf of Thailand are situated in pre-deformed lithospheric segments such as the Inthanon zone and Sukhothai Arc that have been deformed during the Indosinian Orogeny (Fig. 2a and b). This zone experienced a new phase of metamorphism in the Late Cretaceous–Eocene as a result of the Andean-type subduction west of Sibumasu (Searle *et al.* 2007; Gardiner *et al.* 2015), and therefore probably lost most of its lithospheric strength. The second requirement (i.e. the rotational extensional stress component) initiated in the late Eocene owing to slab pull forces at the Java–Sunda–Sumatra subduction zone since 45 Ma (Hall 2009), as India was obliquely colliding with Eurasia at that time. The influence of inherited orogenic structures on hot continental lithosphere undergoing extensional forces was investigated in a 2D numerical modelling approach by Balàzs *et al.* (2017). Those researchers modelled the effect of a lithospheric weak zone, representing a subducted slab of oceanic lithosphere, in the lithospheric mantle and subsequently calculated strain patterns in the lithosphere. The 2D geometry of the intracontinental rift basins caused by these extensional forces that would develop could be predicted. Extensional forces affecting the weakened lithosphere resulted in the development of sedimentary basins with normal synrift and post-rift evolution, but also in the development of some sedimentary basins with extreme amounts of post-rift subsidence. This situation of extreme post-rift subsidence is well described in the Pattani, Kra and Northern Malay basin in the eastern Gulf of Thailand (Tjia 1994; Ngah *et al.* 1996; Morley & Westaway 2006; Morley & Racey 2011). The strain-based 2D modelling of Balàzs *et al.* (2017) showed that the presence of pre-existing orogenic structures in hot lithosphere causes the development of (1) asymmetric half-graben development bound by low-angle normal faults during synrift evolution, (2) high post-rift subsidence in some of the developed basins, (3) asymmetrical asthenospheric upwelling leading to delayed mafic alkaline magmatism during the post-rift phase and (4) uplift during initial extension and syn- to post-rift transition (Balàzs *et al.* 2017). This last feature in particular comes into play when interpreting our data. The presented low-temperature thermochronological data (especially for sample KM-04) indicate that tectonic exhumation along low-angle normal faults occurred during initial extension in the region (in approximately late Eocene time) (Tables 3 and 4). The episodes of basin inversion around the Oligocene–Miocene transition (*c.* 23 Ma) also indicate significant exhumation on- and offshore during syn- to post-rift phase progression. Hence, these similarities show that the 2D strain-based modelling approach of Balàzs *et al.* (2017) has great potential and seems to be applicable in Thailand (and maybe the whole of SE Asia) for improving our understanding on basin development and in particular the anomalous features that characterize the Gulf of Thailand (e.g. as reviewed by Morley 2015).

Further underscoring the broader implications of our observations, recent 3D strain-based modelling by Le Pourhiet *et al.* (2018) investigating the opening and propagation of the South China Sea explained the V-shaped nature of the oceanic rift by the influence of far-field tectonic effects. Moreover, their modelling predicted that the width of the rift basins increased towards the propagator (Le Pourhiet *et al.* 2018), which is certainly the case for the Gulf of Thailand (Fig. 8). Strike-slip faults at an angle of 45° to the direction of extension typically bound these rift basins (Le Pourhiet *et al.* 2018). These observations from this theoretical 3D model are comparable with the geometries of the rift basins characteristic of the eastern Gulf of Thailand (i.e. west of the South China Sea), which opened in the late Eocene and continued rifting until the late Oligocene. Numerous faults such as the Mae Ping and Three Pagodas Faults trend NW–SE whereas the Ranong and Khlong Marui Fault zones trend NE–SW; these trends are both at 45° to the east–west extensional direction in which the failed rift basins developed. A drastic change in spreading direction by 15° owing to far-field tectonic driving forces occurred in the South China Sea at magnetic anomaly 6a (i.e. at 20.5 Ma) (Sibuet *et al.* 2016), which is contemporaneous with the transition to a post-rift phase of the basin of the eastern Gulf of Thailand (Fig. 8, right panel).

Conclusions

Based on our new low-temperature thermochronological data and thermal history modelling on basement rocks in southeastern Thailand, we can draw the following conclusions.

(1) The basement rocks of southeastern Thailand experienced exhumation predominantly during the Late Eocene and Oligocene. Most apatite fission-track and (U–Th)/He ages concentrate around 36–24 Ma, which is in agreement with previous estimates of the timing of exhumation along the major Mae Ping and Three Pagodas Fault zones. These estimates are related to late Eocene sinistral displacement along the Mae Ping and Three Pagodas Fault zones, as already observed in western Thailand and southern Vietnam. During the late Oligocene, some of the sampled rocks experienced final cooling as a result of the minor dextral motion along the Mae Ping and Three Pagodas Fault zones.The synrift phase (Late Eocene to the Oligocene–Miocene transition) of the failed rift basins of the eastern Gulf of Thailand occurred simultaneously with onshore basement cooling and thus exhumation through the upper crust of southeastern Thailand.

(2) Exhumation decreased in southeastern Thailand after the Oligocene–Miocene transition (*c.* 23 Ma), under the influence of a changing regional stress pattern caused by larger-scale plate-tectonic events in Sundaland. Specifically in the eastern Gulf of Thailand the change of the regional stress patterns is related to the cessation of rifting, and onset of thermal subsidence at around 23 Ma. Promising similarities between model and ground-truthing indicate that results from thermochronological studies should possibly be incorporated in lithospheric strain modelling studies to further test the geological reality with the model's predicted time-slices.

Acknowledgements We would like to thank P. Surakiatchai, who assisted during fieldwork. We are very grateful to A.-E. Debeer for assistance in the laboratory during mineral separations. J. Schwanethal is acknowledged for development and maintenance of the apatite (U–Th)/He facilities at UCL. We would like to thank B. Van Houdt and G. Vittiglio for help during neutron irradiation at the Belgian Nuclear Research Centre in Mol (SCK-CEN, BR1 facility). We would like to thank W. Xiao for editorial work. This paper benefited from many useful suggestions from two anonymous referees, for which we are very grateful.

Funding S.N. received a PhD Fellowship of the Research Foundation – Flanders (FWO). Funding for J.D.G. was from a research grant from the Research Foundation – Flanders (FWO) number 31528111. S.G.'s contribution was supported by an Australian Research Council Discovery grant (DP150101730) and forms TRAX record 418. P.K. was funded by Ratchadaphiseksomphot Endowment Fund, Chulalongkorn University.

Author contributions SMN: Conceptualization (Lead), Funding acquisition (Equal), Investigation (Lead), Methodology (Lead), Visualization (Lead), Writing – Original Draft (Lead), Writing – Review & Editing (Lead); SG: Supervision (Supporting), Writing – Review & Editing (Equal); CM: Conceptualization (Equal), Visualization (Equal), Writing – Review & Editing (Equal); PC: Investigation (Supporting), Writing – Review & Editing (Supporting); PK: Funding acquisition (Supporting), Resources (Supporting); PV: Methodology (Equal), Software (Lead), Writing – Review & Editing (Supporting); AC: Methodology (Equal), Writing – Review & Editing (Supporting); GVR: Methodology (Equal), Writing – Review & Editing (Supporting); JDG: Funding acquisition (Equal), Project administration (Equal), Supervision (Lead), Writing – Review & Editing (Lead)

Scientific editing by Wenjiao Xiao

References

Balàzs, A., Burov, E., Matenco, L., Vogt, K., Francois, T. & Cloetingh, S. 2017. Symmetry during the syn- and post-rift evolution of extensional back-arc basins: The role of inherited orogenic structures. *Earth and Planetary Science Letters*, **462**, 86–98, https://doi.org/10.1016/j.epsl.2017.01.015

Barbarand, J., Carter, A., Wood, I. & Hurford, T. 2003. Compositional and structural control of fission-track annealing in apatite. *Chemical Geology*, **198**, 107–137, https://doi.org/10.1016/S0009-2541(02)00424-2

Barber, A.J., Ridd, M.F. & Crow, M.J. 2011. The origin, movement and assembly of the pre-Tertiary tectonic units of Thailand. *In*: Ridd, M.F., Barber, A.J. & Crow, M.J. (eds) *The Geology of Thailand*. Geological Society, London, 507–537.

Blomme, K. 2013. *Apatite fission track thermochronology and petrographic characterization of south Thailand granitoids: evolution of the Andaman Basin with respect to the eastern Indian passive margin*. MSc thesis, Ghent University.

Charusiri, P., Clark, A.H., Farrar, E., Archibald, D. & Charusiri, B. 1993. Granite belts in Thailand: evidence from $^{40}Ar/^{39}Ar$ geochronological and geological syntheses. *Journal of Southeast Asian Earth Sciences*, **8**, 127–136, https://doi.org/10.1016/0743-9547(93)90014-G

Cobbing, E.J. 1992. *The Granites of the South-East Asian Tin Belt*. HMSO, London.

Cobbing, E.J. 2011. Granitic rocks. *In*: Ridd, M.F., Barber, A.J. & Crow, M.J. (eds) *The Geology of Thailand*. Geological Society, London, 441–457.

Cottam, M.A., Hall, R. & Ghani, A.A. 2013. Late Cretaceous and Cenozoic tectonics of the Malay Peninsula constrained by thermochronology. *Journal of Asian Earth Sciences*, **76**, 241–257, https://doi.org/10.1016/j.jseaes.2013.04.029

Crow, M.J. 2011. Appendix. Radiometric ages of Thailand rocks. *In*: Ridd, M.F., Barber, A.J. & Crow, M.J. (eds) *The Geology of Thailand*. Geological Society, London, 593–614.

De Corte, F., Bellemans, F., Van den haute, P., Ingelbrecht, C. & Nicholl, C. 1998. A new U doped glass certified by the European Commission for the calibration of fission-track dating. *In*: Van den haute, P., de Corte, F. (eds) *Advances in fission-track geochronology*. Springer, Dordrecht, 67–78, https://doi.org/10.1007/978-94-015-9133-1_5

De Grave, J. & Van den haute, P. 2002. Denudation and cooling of the Lake Teletskoye Region in the Altai Mountains (South Siberia) as revealed by apatite fission-track thermochronology. *Tectonophysics*, **349**, 145–159, https://doi.org/10.1016/S0040-1951(02)00051-3

De Grave, J., Buslov, M.M., Van den haute, P., Dehandschutter, B. & McWilliams, M.O. 2009. Multi-method chronometry of the Teletskoye graben and its basement, Siberian Altai Mountains: new insights on its thermo-tectonic evolution. *In*: Lisker, F., Ventura, B. & Glasmacher, U.A. (eds) *Thermochronological Methods: From Palaeotemperature Constraints to Landscape Evolution Models*. Geological Society, London, Special Publications, **324**, 237–259, https://doi.org/10.1144/SP324.17

De Grave, J., Glorie, S., Vermaercke, P., Vittiglio, G. & Van den haute, P. 2010. A 'new' irradiation facility for FT applications at the Belgian Nuclear Research Centre: the BR1 reactor. *In*: *Thermo 2010*.

De Grave, J., Glorie, S., *et al.* 2011. The thermo-tectonic history of the Song-Kul plateau, Kyrgyz Tien Shan: Constraints by apatite and titanite thermochronometry and zircon U/Pb dating. *Gondwana Research*, **20**, 745–763, https://doi.org/10.1016/j.gr.2011.03.011

Department of Mineral Fuels, Ministry of Energy. 2018. Information memorandum, Thailand petroleum bidding round 2018 for offshore block G1/61&G2/61, Attachment 4, http://bidding2018.dmf.go.th/G2/images/doc/IM_EN_Final.pdf

Dew, R.E.C., Collins, A.S., *et al.* 2018*a*. Probing into Thailand's basement: New insights from U–Pb geochronology, Sr, Sm–Nd, Pb and Lu–Hf isotopic systems from granitoids. *Lithos*, **320–321**, 332–354, https://doi.org/10.1016/j.lithos.2018.09.019

Dew, R.E.C., Nachtergaele, S., *et al.* 2018*b*. Data analysis of the U–Pb geochronology and Lu–Hf system in zircon and whole-rock Sr, Sm–Nd and Pb isotopic systems for the granitoids of Thailand. *Data in Brief*, **21**, 1794–1809, https://doi.org/10.1016/j.dib.2018.10.176

Donelick, R.A. 1993. Apatite etching characteristics versus chemical composition. *Nuclear Tracks and Radiation Measurements*, **96**, 62–66, https://doi.org/US005485919A

Donelick, R.A. & Miller, D.S. 1991. Enhanced TINT fission track densities in low spontaneous track density apatites using ^{252}Cf-derived fission fragment tracks: a model and experimental observations. *Nuclear Tracks and Radiation Measurements*, **18**, 301–307, https://doi.org/10.1016/1359-0189(91)90022-A

Ehlers, T.A. & Farley, K.A. 2003. Apatite (U–Th)/He thermochronometry: methods and applications to problems in tectonic and surface processes. *Earth and Planetary Science Letters*, **206**, 1–14, https://doi.org/10.1016/S0012-821X(02)01069-5

Enkelmann, E., Jonckheere, R. & Ratschbacher, L. 2005. Absolute measurements of the uranium concentration in thick samples using fission-track detectors. *Nuclear Instruments and Methods in Physics Research Section B: Beam Interactions with Materials and Atoms*, **229**, 489–498.

Flowers, R.M., Farley, K.A. & Ketcham, R.A. 2015. A reporting protocol for thermochronologic modeling illustrated with data from the Grand Canyon. *Earth and Planetary Science Letters*, **432**, 425–435, https://doi.org/10.1016/j.epsl.2015.09.053

François, T., Md Ali, M.A., Matenco, L., Willingshofer, E., Ng, T.F., Taib, N.I. & Shuib, M.K. 2017. Late Cretaceous extension and exhumation of the Stong and Taku magmatic and metamorphic complexes, NE Peninsular Malaysia. *Journal of Asian Earth Sciences*, **143**, 296–314, https://doi.org/10.1016/j.jseaes.2017.04.009

Fyhn, M.B.W., Green, P.F., *et al.* 2016. Cenozoic deformation and exhumation of the Kampot Fold Belt and implications for south Indochina tectonics. *Journal of Geophysical Research: Solid Earth*, **121**, 5278–5307, https://doi.org/10.1002/2016JB012847

Galbraith, R.F. 1990. The radial plot: Graphical assessment of spread in ages. *International Journal of Radiation Applications and Instrumentation, Part D* , **17**, 207–214, https://doi.org/10.1016/1359-0189(90)90036-w

Gallagher, K. 2012. Transdimensional inverse thermal history modeling for quantitative thermochronology. *Journal of Geophysical Research: Solid Earth*, **117**, 1–16, https://doi.org/10.1029/2011JB008825

Gallagher, K. 2016. Comment on 'A reporting protocol for thermochronologic modeling illustrated with data from the Grand Canyon' by Flowers, Farley and Ketcham. *Earth and Planetary Science Letters*, **441**, 211–212, https://doi.org/10.1016/j.epsl.2016.02.021

Gardiner, N.J., Searle, M.P., Robb, L.J. & Morley, C.K. 2015. Neo-Tethyan magmatism and metallogeny in Myanmar – An Andean analogue? *Journal of Asian Earth Sciences*, **106**, 197–215, https://doi.org/10.1016/j.jseaes.2015.03.015

Gardiner, N.J., Searle, M.P., Morley, C.K., Whitehouse, M.P., Spencer, C.J. & Robb, L.J. 2016. The closure of Palaeo-Tethys in Eastern Myanmar and Northern Thailand: New insights from zircon U–Pb and Hf isotope data. *Gondwana Research*, **39**, 401–422, https://doi.org/10.1016/j.gr.2015.03.001

Geard, A. 2008. *Geology of the Klaeng Region (southeast Thailand): lithology, structure and geochronology*. BSc Hons thesis, University of Tasmania, Hobart.

Gleadow, A.J.W., Duddy, I.R., Green, P.F. & Lovering, J.F. 1986. Confined fission track lengths in apatite: a diagnostic tool for thermal history analysis. *Contributions to Mineralogy and Petrology*, **94**, 405–415, https://doi.org/10.1007/BF00376334

Glorie, S., De Grave, J., Buslov, M.M., Elburg, M.A., Stockli, D.F., Gerdes, A. & Van den haute, P. 2010. Multi-method chronometric constraints on the evolution of the Northern Kyrgyz Tien Shan granitoids (Central Asian Orogenic Belt): From emplacement to exhumation. *Journal of Asian Earth Sciences*, **38**, 131–146, https://doi.org/10.1016/j.jseaes.2009.12.009

Green, P. & Duddy, I. 2018. Apatite (U–Th–Sm)/He thermochronology on the wrong side of the tracks. *Chemical Geology*, **488**, 21–33, https://doi.org/10.1016/j.chemgeo.2018.04.028

Green, P.F., Duddy, I.R., Gleadow, A.J.W., Tingate, P.R. & Laslett, G.M. 1986. Thermal annealing of fission tracks in apatite 1. A qualitative description. *Chemical Geology*, **59**, 237–253, https://doi.org/10.1016/0168-9622(86)90074-6

Hall, R. 2009. Hydrocarbon basins in SE Asia: understanding why they are there. *Petroleum Geoscience*, **15**, 131–146, https://doi.org/10.1144/1354-079309-830

Heward, A.P., Chuenbunchom, S., Mäkel, G., Marsland, D. & Spring, L. 2000. Nang Nuan oil field, B6/27, Gulf of Thailand: karst reservoirs of meteoric or deep-burial origin. *Petroleum Geoscience*, **6**, 15–27, https://doi.org/10.1144/petgeo.6.1.15

Hurford, A.J. 1990. Standardization of fission track dating calibration: Recommendation by the Fission Track Working Group of the I.U.G.S. Subcommission on Geochronology. *Chemical Geology*, **80**, 171–178, https://doi.org/10.1016/0168-9622(90)90025-8

Hurford, A.J. & Green, P.F. 1983. The zeta age calibration of fission-track dating. *Chemical Geology*, **41**, 285–317, https://doi.org/10.1016/S0009-2541(83)80026-6

Hutchison, C.S. 1975. Ophiolite in Southeast Asia. *Geological Society of America Bulletin*, **86**, 797–806, https://doi.org/10.1130/0016-7606(1975)86<797:OISA>2.0.CO;2

Hutchison, C.S. 1977. Granite emplacement and tectonic subdivision of Peninsular Malaysia. *Bulletin of the Geological Society of Malaysia*, **9**, 187–207, https://doi.org/10.7186/bgsm09197714

Hutchison, C.S. 2007. *Geological Evolution of South-East Asia*. Geological Society of Malaysia, Kuala Lumpur, https://doi.org/10.1016/0264-8172(91)90051-2

Kanjanapayont, P., Klötzli, U., Thöni, M., Grasemann, B. & Edwards, M.A. 2012. Rb–Sr, Sm–Nd, and U–Pb geochronology of the rocks within the Khlong Marui shear zone, southern Thailand. *Journal of Asian Earth Sciences*, **56**, 263–275, https://doi.org/10.1016/j.jseaes.2012.05.029

Kanjanapayont, P., Kieduppatum, P., Klötzli, U., Klötzli, E. & Charusiri, P. 2013. Deformation history and U–Pb zircon geochronology of the high grade metamorphic rocks within the Klaeng fault zone, eastern Thailand. *Journal of Asian Earth Sciences*, **77**, 224–233, https://doi.org/10.1016/j.jseaes.2013.08.027

Kawakami, T., Nakano, N., *et al.* 2014. U–Pb zircon and CHIME monazite dating of granitoids and high-grade metamorphic rocks from the Eastern and Peninsular Thailand – A new report of Early Paleozoic granite. *Lithos*, **200–201**, 64–79, https://doi.org/10.1016/j.lithos.2014.04.012

Ketcham, R.A., Donelick, R.A. & Carlson, W.D. 1999. Variability of apatite fission-track annealing kinetics: III. Extrapolation to geological time scales. *American Mineralogist*, **84**, 1235–1255, https://doi.org/10.2138/am-1999-0903

Ketcham, R.A., Carter, A., Donelick, R.A., Barbarand, J. & Hurford, A.J. 2007*a*. Improved measurement of fission-track annealing in apatite using *c*-axis projection. *American Mineralogist*, **92**, 789–798, https://doi.org/10.2138/am.2007.2280

Ketcham, R.A., Carter, A., Donelick, R.A., Barbarand, J. & Hurford, A.J. 2007*b*. Improved modeling of fission-track annealing in apatite. *American Mineralogist*, **92**, 799–810, https://doi.org/10.2138/am.2007.2281

Ketcham, R.A., Gautheron, C. & Tassan-Got, L. 2011. Accounting for long alpha-particle stopping distances in (U–Th–Sm)/He geochronology: Refinement of the baseline case. *Geochimica et Cosmochimica Acta*, **75**, 7779–7791, https://doi.org/10.1016/j.gca.2011.10.011

Krähenbuhl, R. 1991. Magmatism, tin mineralization and tectonics of the Main Range, Malaysian Peninsula: Consequences for the plate tectonic model of Southeast Asia based on Rb–Sr, K–Ar and fission track data. *Bulletin of the Geological Society of Malaysia*, **29**, 1–100, https://doi.org/10.7186/bgsm29199101

Lacassin, R., Maluski, H., *et al.* 1997. Tertiary diachronic extrusion and deformation of western Indochina: structural and $^{40}Ar/^{39}Ar$ evidence from NW Thailand. *Journal of Geophysical Research*, **102**, https://doi.org/10.1029/96JB03831

Le Pourhiet, L., Chamot-Rooke, N., Delescluse, M., May, D.A., Watremez, L. & Pubellier, M. 2018. Continental break-up of the South China Sea stalled by far-field compression. *Nature Geoscience*, **11**, 1–5, https://doi.org/10.1038/s41561-018-0178-5

Lepvrier, C., Maluski, H., Van Tich, V., Leyreloup, A., Truong Thi, P. & Van Vuong, N. 2004. The Early Triassic Indosinian orogeny in Vietnam (Truong Son Belt and Kontum Massif); implications for the geodynamic evolution of Indochina. *Tectonophysics*, **393**, 87–118, https://doi.org/10.1016/j.tecto.2004.07.030

Md Ali, M.A., Willingshofer, E., *et al.* 2016. Kinematics of post-orogenic extension and exhumation of the Taku Schist, NE Peninsular Malaysia. *Journal of Asian Earth Sciences*, **127**, 63–75, https://doi.org/10.1016/j.jseaes.2016.06.020

Metcalfe, I. 1996. Pre-Cretaceous evolution of SE Asian terranes. *In:* Hall, R. & Blundell, D. (eds) *Tectonic Evolution of Southeast Asia*. Geological Society, London, Special Publications, **106**, 97–122, https://doi.org/10.1144/GSL.SP.1996.106.01.09

Metcalfe, I. 2000. The Bentong–Raub Suture Zone. *Journal of Asian Earth Sciences*, **18**, 691–712, https://doi.org/10.1016/S1367-9120(00)00043-2

Metcalfe, I. 2011. Tectonic framework and Phanerozoic evolution of Sundaland. *Gondwana Research*, **19**, 3–21, https://doi.org/10.1016/j.gr.2010.02.016

Metcalfe, I. 2013. Gondwana dispersion and Asian accretion: Tectonic and palaeogeographic evolution of eastern Tethys. *Journal of Asian Earth Sciences*, **66**, 1–33, https://doi.org/10.1016/j.jseaes.2012.12.020

Mitchell, A.H. 1977. Tectonic settings for emplacement of southeast Asian tin granites. *Bulletin of the Geological Society of Malaysia*, **9**, 123–140, https://doi.org/10.7186/bgsm09197710

Molnar, N.E., Cruden, A.R. & Betts, P.G. 2018. Unzipping continents and the birth of microcontinents. *Geology*, **46**, 451–454, https://doi.org/10.1130/G40021.1

Morley, C.K. 2002. A tectonic model for the Tertiary evolution of strike-slip faults and rift basins in SE Asia. *Tectonophysics*, **347**, 189–215, https://doi.org/10.1016/S0040-1951(02)00061-6

Morley, C.K. 2004. Nested strike -slip duplexes, and other evidence for Late Cretaceous - Paleogene transpressional tectonics before and during India -Eurasia collision, in Thailand, Myanmar and Malaysia. *Journal of the Geological Society, London*, **161**, 799–812, https://doi.org/10.1144/0016-764903-124

Morley, C.K. 2012. Late Cretaceous–Early Palaeogene tectonic development of SE Asia. *Earth-Science Reviews*, **115**, 37–75, https://doi.org/10.1016/j.earscirev.2012.08.002

Morley, C.K. 2015. Five anomalous structural aspects of rift basins in Thailand and their impact on petroleum systems. *In*: Richards, F.L., Richardson, N.J., Rippington, S.J., Wilson, R.W. & Bond, C.E. (eds) *Industrial Structural Geology: Principles, Techniques and Integration*. Geological Society, London, Special Publications, **421**, 143–168, https://doi.org/10.1144/SP421.2

Morley, C.K. 2017. Cenozoic rifting, passive margin development and strike-slip faulting in the Andaman Sea: a discussion of established v. new tectonic models. *In*: Bandopadhyay, P.C. & Carter, A. (eds) *The Andaman–Nicobar Accretionary Ridge: Geology, Tectonics and Hazards*. Geological Society, London, Memoirs, **47**, 27–50, https://doi.org/10.1144/M47.4

Morley, C.K. 2018. Understanding Sibumasu in the context of ribbon continents. *Gondwana Research*, **64**, 184–215, https://doi.org/10.1016/j.gr.2018.07.006

Morley, C.K. & Arboit, F. 2019. Dating the onset of motion on the Sagaing fault: Evidence from detrital zircon and titanite U–Pb geochronology from the North Minwun Basin, Myanmar. *Geology*, **47**, 581–585, https://doi.org/10.1130/G46321.1

Morley, C.K. & Racey, A. 2011. Tertiary stratigraphy. *In*: Ridd, M.F., Barber, A.J. & Crow, M.J. (eds) *The Geology of Thailand*. Geological Society, London, 223–271.

Morley, C.K. & Westaway, R. 2006. Subsidence in the super-deep Pattani and Malay basins of Southeast Asia: A coupled model incorporating lower-crustal flow in response to post-rift sediment loading. *Basin Research*, **18**, 51–84, https://doi.org/10.1111/j.1365-2117.2006.00285.x

Morley, C.K., Sangkumarn, N., Hoon, T.B., Chonglakmani, C. & Lambiase, J. 2000. Structural evolution of the Li Basin, northern Thailand. *Journal of the Geological Society, London*, **157**, 483–492, https://doi.org/10.1144/jgs.157.2.483

Morley, C.K., Woganan, N., Sankumarn, N., Hoon, T.B., Alief, A. & Simmons, M. 2001. Late Oligocene–Recent stress evolution in rift basins of northern and central Thailand: implications for escape tectonics. *Tectonophysics*, **334**, 115–150, https://doi.org/10.1016/S0040-1951(00)00300-0

Morley, C.K., Haranya, C., Phoosongsee, W., Pongwapee, S., Kornsawan, A. & Wonganan, N. 2004. Activation of rift oblique and rift parallel pre-existing fabrics during extension and their effect on deformation style: examples from the rifts of Thailand. *Journal of Structural Geology*, **26**, 1803–1829, https://doi.org/10.1016/j.jsg.2004.02.014

Morley, C.K., Smith, M., Carter, A., Charusiri, P. & Chantraprasert, S. 2007. Evolution of deformation styles at a major restraining bend, constraints from

cooling histories, Mae Ping fault zone, western Thailand. *In*: Cunningham, W.D. & Mann, P. (eds) *Tectonics of Strike-Slip Restraining and Releasing Bends*. Geological Society, London, Special Publications, **290**, 325–349, https://doi.org/10.1144/SP290.12

Morley, C.K., Charusiri, P. & Watkinson, I. 2011. Structural geology of Thailand during the Cenozoic. *In*: Ridd, M.F., Barber, A.J. & Crow, M.J. (eds) *The Geology of Thailand*. Geological Society, London, 273–334.

Nachtergaele, S., Glorie, S., Charusiri, P., Kanjanapayont, P. & De Grave, J. 2017. Cenozoic exhumation of basement rocks in Thailand: constraints from apatite fission track and apatite (U–Th)/He thermochronology. *In*: 16th Gondwana International Conference, Bangkok, Thailand.

Nachtergaele, S., De Pelsmaeker, E., *et al.* 2018. Meso-Cenozoic tectonic evolution of the Talas–Fergana region of the Kyrgyz Tien Shan revealed by low-temperature basement and detrital thermochronology. *Geoscience Frontiers*, **9**, 1495–1514, https://doi.org/10.1016/j.gsf.2017.11.007

Nantasin, P., Hauzenberger, C., Liu, X., Krenn, K., Dong, Y., Thöni, M. & Wathanakul, P. 2012. Occurrence of the high grade Thabsila metamorphic complex within the low grade Three Pagodas shear zone, Kanchanaburi Province, western Thailand: Petrology and geochronology. *Journal of Asian Earth Sciences*, **60**, 68–87, https://doi.org/10.1016/j.jseaes.2012.07.025

Ngah, K., Madon, M. & Tjia, H.D. 1996. Role of pre-Tertiary fractures in formation and development of the Malay and Penyu basins. *In:*Hall, R. & Blundell, E. (eds) *Tectonic Evolution of Southeast Asia*. Geological Society, London, Special Publications, **106**, 281–289, https://doi.org/10.1144/GSL.SP.1996.106.01.18

Pal, T. 2011. Petrology and geochemistry of the Andaman ophiolite: melt–rock interaction in a suprasubduction-zone setting. *Journal of the Geological Society, London*, **168**, 1031–1045, https://doi.org/10.1144/0016-76492009-152

Palin, R.M., Searle, M.P., Morley, C.K., Charusiri, P., Horstwood, M.S.A. & Roberts, N.M.W. 2013. Timing of metamorphism of the Lansang gneiss and implications for left-lateral motion along the Mae Ping (Wang Chao) strike-slip fault, Thailand. *Journal of Asian Earth Sciences*, **76**, 120–136, https://doi.org/10.1016/j.jseaes.2013.01.021

Pedersen, R.B., Searle, M.P., Carter, A. & Bandopadhyay, P.C. 2010. U–Pb zircon age of the Andaman ophiolite: implications for the beginning of subduction beneath the Andaman–Sumatra arc. *Journal of the Geological Society, London*, **167**, 1105–1112, https://doi.org/10.1144/0016-76492009-151

Pubellier, M. & Morley, C.K. 2014. The basins of Sundaland (SE Asia): Evolution and boundary conditions. *Marine and Petroleum Geology*, **58**, 555–578, https://doi.org/10.1016/j.marpetgeo.2013.11.019

Putthapiban, P. 1984. *Geochemistry, geochronology and tin mineralization*. PhD thesis, Chiang Mai University, Chiang Mai.

Qian, X., Feng, Q., Wang, Y., Zhao, T., Zi, J.W., Udchachon, M. & Wang, Y. 2017. Late Triassic post-collisional granites related to Paleotethyan evolution in SE Thailand: Geochronological and geochemical constraints. *Lithos*, **286–287**, 440–453, https://doi.org/10.1016/j.lithos.2017.06.026

Racey, A. 2011. Petroleum geology. *In*: Ridd, M.F., Barber, A.J. & Crow, M.J. (eds) *The Geology of Thailand*. Geological Society, London, 351–392.

Racey, A., Duddy, I.R. & Love, M.A. 1997. Apatite fission track analysis of Mesozoic red beds from northeastern Thailand and western Laos. *In*: The International Conference on Stratigraphy and Tectonic Evolution of Southeast Asia and the South Pacific, Bangkok, Thailand, 19–24 August 1997, 200–209.

Ridd, M.F. 2009. The Phuket Terrane: A Late Palaeozoic rift at the margin of Sibumasu. *Journal of Asian Earth Sciences*, **36**, 238–251, https://doi.org/10.1016/j.jseaes.2009.06.006

Ridd, M.F. 2012. The role of strike-slip faults in the displacement of the Palaeotethys suture zone in Southeast Thailand. *Journal of Asian Earth Sciences*, **51**, 63–84, https://doi.org/10.1016/j.jseaes.2012.01.018

Ridd, M.F. 2015. East flank of the Sibumasu block in NW Thailand and Myanmar and its possible northward continuation into Yunnan: A review and suggested tectono-stratigraphic interpretation. *Journal of Asian Earth Sciences*, **104**, 160–174, https://doi.org/10.1016/j.jseaes.2014.01.023

Ridd, M.F. & Morley, C.K. 2011. The Khao Yai Fault on the southern margin of the Khorat Plateau, and the pattern of faulting in Southeast Thailand. *Proceedings of the Geologists' Association*, **122**, 143–156, https://doi.org/10.1016/j.pgeola.2010.08.008

Sautter, B., Pubellier, M., Jousselin, P., Dattilo, P., Kerdraon, Y., Choong, C.M. & Menier, D. 2017. Late Paleogene rifting along the Malay Peninsula thickened crust. *Tectonophysics*, **710–711**, 205–224, https://doi.org/10.1016/j.tecto.2016.11.035

Schmidt, W.J., Hoang, B.H., Handschy, J.W. & Hai, V.T. 2019. Tectonic evolution and regional setting of the Cuu Long Basin, Vietnam. *Tectonophysics*, **757**, 36–57, https://doi.org/10.1016/j.tecto.2019.03.001

Searle, M.P. & Morley, C.K. 2011. Tectonic and thermal evolution of Thailand in the regional context of SE Asia. *In*: Ridd, M.F., Barber, A.J. & Crow, M.J. (eds) *The Geology of Thailand*. Geological Society, London, 539–571.

Searle, M.P., Noble, S.R., Cottle, J.M., Waters, D.J., Mitchell, A.H.G., Hlaing, T. & Horstwood, M.S.A. 2007. Tectonic evolution of the Mogok metamorphic belt, Burma (Myanmar) constrained by U–Th–Pb dating of metamorphic and magmatic rocks. *Tectonics*, **26**, https://doi.org/10.1029/2006TC002083

Searle, M.P., Whitehouse, M.J., *et al.* 2012. Tectonic evolution of the Sibumasu–Indochina terrane collision zone in Thailand and Malaysia: constraints from new U–Pb zircon chronology of SE Asian tin granitoids. *Journal of the Geological Society, London*, **169**, 489–500, https://doi.org/10.1144/0016-76492011-107

Sibuet, J.C., Yeh, Y.C. & Lee, C.S. 2016. Geodynamics of the South China Sea. *Tectonophysics*, **692**, 98–119, https://doi.org/10.1016/j.tecto.2016.02.022

Simons, W.J.F., Socquet, A., *et al.* 2007. A decade of GPS in Southeast Asia: Resolving Sundaland motion and boundaries. *Journal of Geophysical Research: Solid Earth*, B06420,112. https://doi.org/10.1029/2005JB003868

Smith, M., Chantraprasert, S., Morley, C.K. & Cartwright, I. 2007. Structural geometry and timing of deformation in the Chainat duplex, Thailand. *In*: Cunningham, W.D. & Mann, P. (eds) *Tectonics of Strike-Slip Restraining and Releasing Bends*. Geological Society, London, Special Publications, **290**, 305–323, https://doi.org/10.1144/SP290.11

Sone, M. & Metcalfe, I. 2008. Parallel Tethyan sutures in mainland Southeast Asia: New insights for Palaeo-Tethys closure and implications for the Indosinian orogeny. *Comptes Rendus Géoscience*, **340**, 166–179, https://doi.org/10.1016/j.crte.2007.09.008

Sone, M., Metcalfe, I. & Chaodumrong, P. 2012. The Chanthaburi terrane of southeastern Thailand: Stratigraphic confirmation as a disrupted segment of the Sukhothai Arc. *Journal of Asian Earth Sciences*, **61**, 16–32, https://doi.org/10.1016/j.jseaes.2012.08.021

Srisuriyon, K. & Morley, C.K. 2014. Pull-apart development at overlapping fault tips: Oblique rifting of a Cenozoic continental margin, northern Mergui Basin, Andaman Sea. *Geosphere*, **10**, 80–106, https://doi.org/10.1130/GES00926.1

Stockli, D.F., Farley, K.A. & Dumitru, T.A. 2000. Calibration of the apatite (U–Th)/He thermochronometer on an exhumed fault block, White Mountains, California. *Geology*, **28**, 983–986, https://doi.org/10.1130/0091-7613(2000)28<983:COTAHT>2.0.CO;2

Tingay, M., Morley, C., King, R., Hillis, R., Coblentz, D. & Hall, R. 2010. Present-day stress field of Southeast Asia. *Tectonophysics*, **482**, 92–104, https://doi.org/10.1016/j.tecto.2009.06.019

Tjia, H.D. 1994. Inversion tectonics in the Malay Basin: evidence and timing of events. *Bulletin of the Geological Society of Malaysia*, **56**, 119–126.

Upton, D. 1999. *A regional fission track study in Thailand: implications for thermal history and denudation*. PhD thesis, Birkbeck and University College London.

Van Ranst, G., Pedrosa-Soares, A.C., Novo, T., Vermeesch, P. & De Grave, J. 2019. New insights from low-temperature thermochronology into the tectonic and geomorphologic evolution of the south-eastern Brazilian highlands and passive margin. *Geoscience Frontiers*, https://doi.org/10.1016/j.gsf.2019.05.011

Vermeesch, P. 2009. RadialPlotter: A Java application for fission track, luminescence and other radial plots. *Radiation Measurements*, **44**, 409–410, https://doi.org/10.1016/j.radmeas.2009.05.003

Vermeesch, P. 2018. IsoplotR: a free and open toolbox for geochronology. *Geoscience Frontiers*, **9**, 1479–1493, https://doi.org/10.1016/j.gsf.2018.04.001

Wagner, G.A. & Van den haute, P. 1992. *Fission-Track Dating*. Springer, Berlin.

Watkinson, I., Elders, C. & Hall, R. 2008. The kinematic history of the Khlong Marui and Ranong Faults, southern Thailand. *Journal of Structural Geology*, **30**, 1554–1571, https://doi.org/10.1016/j.jsg.2008.09.001

Watkinson, I., Elders, C., Batt, G., Jourdan, F., Hall, R. & McNaughton, N.J. 2011. The timing of strike-slip shear along the Ranong and Khlong Marui faults, Thailand. *Journal of Geophysical Research: Solid Earth*, **116**, 1–26, https://doi.org/10.1029/2011JB008379.

Wildman, M., Brown, R., *et al.* 2017. Contrasting Mesozoic evolution across the boundary between on and off craton regions of the South African plateau inferred from apatite fission track and (U–Th–Sm)/He thermochronology. *Journal of Geophysical Research: Solid Earth*, **122**, 1517–1547, https://doi.org/10.1002/2016JB013478

Zeitler, P., Herczeg, A.L., Mcdougall, I. & Honda, M. 1987. U–Th–He dating of apatite: a potential thermochronometer. *Geochimica et Cosmochimica Acta*, **51**, 2865–2868, https://doi.org/10.1016/0016-7037(87)90164-5